




RESEARCH PAPER



Synthesis, biological evaluation, and *in silico* studies of new CDK2 inhibitors based on pyrazolo[3,4-*d*]pyrimidine and pyrazolo[4,3-*e*][1,2,4]triazolo[1,5-*c*]pyrimidine scaffold with apoptotic activity

Asmaa A. Mandour^a, Ibrahim F. Nassar^b , Mohammed T. Abdel Aal^c, Mahmoud A. E. Shahin^c, Wael A. El-Sayed^{d,e} , Maghawry Hegazy^f, Amr Mohamed Yehia^f, Ahmed Ismail^f, Mohamed Hagra^g, Eslam B. Elkaeed^h, Hanan M. Refaat^a and Nasser S. M. Ismail^a 

^aPharmaceutical Chemistry Department, Faculty of Pharmacy, Future University in Egypt (FUE), Cairo, Egypt; ^bFaculty of Specific Education, Ain Shams University (ASU), Cairo, Egypt; ^cChemistry Department, Faculty of Science, Menoufia University, Shebin El-Kom, Egypt; ^dChemistry Department, College of Science, Qassim University, Qassim, Saudi Arabia; ^ePhotochemistry Department, National Research Centre, Cairo, Egypt; ^fBiochemistry and Molecular Biology Department, Faculty of Pharmacy (Boys), Al-Azhar University, Cairo, Egypt; ^gDepartment of Pharmaceutical Organic Chemistry, College of Pharmacy (Boys), Al-Azhar University, Cairo, Egypt; ^hDepartment of Pharmaceutical Science, College of Pharmacy, Al Maarefa University, Riyadh, Saudi Arabia

ABSTRACT

Cyclin-dependent kinase inhibition is considered a promising target for cancer treatment for its crucial role in cell cycle regulation. Pyrazolo pyrimidine derivatives were well established for their antitumor activity via CDK2 inhibition. In this research, new series of pyrazolopyrimidine derivatives (**4–15**) was designed and synthesised as novel CDK2 inhibitors. The anti-proliferative activities against MCF-7, HCT-116, and HepG-2 were used to evaluate their anticancer activity as novel CDK2 inhibitors. Most of the compounds showed superior cytotoxic activity against MCF-7 and HCT-116 compared to Sorafenib. Only compounds **8**, **14**, and **15** showed potent activity against HepG-2. The CDK2/cyclin A2 enzyme inhibitory activity was tested for all synthesised compounds. Compound **15** showed the most significant inhibitory activity with IC_{50} $0.061 \pm 0.003 \mu\text{M}$. It exerted remarkable alteration in Pre G1 and S phase cell cycle progression and caused apoptosis in HCT cells. In addition, the normal cell line cytotoxicity for compound **15** was assigned revealing low cytotoxic results in normal cells rather than cancer cells. Molecular docking was achieved on the designed compounds and confirmed the two essential hydrogen binding with Leu83 in CDK2 active site. *In silico* ADMET studies and drug-likeness showed proper pharmacokinetic properties which helped in structure requirements prediction for the observed antitumor activity.

ARTICLE HISTORY

Received 5 April 2022
Revised 23 May 2022
Accepted 1 June 2022

KEYWORDS

Pyrazolopyrimidine; CDK2; apoptosis; cytotoxicity; ADMET



1. Introduction

Protein kinases represent a large group of structurally related enzymes that are essential and regulate cell cycle progression involved in cell division^{1–3}. Cyclin-dependent kinases (CDKs) are serine-threonine kinases responsible for cell cycle regulation and cell differentiation². Cyclin-dependent kinases (CDK) are mainly responsible for the phosphorylation process of proteins^{4–6}. Cyclin is the regulatory protein bound by CDK leading to ATP binding region modification². CDKs in absence of cyclin have less activity where the activation loop (known as T-loop) blocks the cleft, and the key amino acid residues are not optimally positioned for ATP binding². CDK2 has a catalytic effect in cyclin-dependent protein kinase complex^{7,8}. Protein phosphorylation has a critical role in cellular function regulation. This essential role during the cell cycle could be altered in tumour cells^{7–11}. Alteration in kinases may lead to the development of many diseases, including cancer. Hence, the control of CDK dependent cell cycle is essential for tumour progression management. Where overexpression of CDK

enzymes occurs in cancer². As uncontrolled CDK2 activation in human cancer is associated with overexpression of cyclins A and E in many human cancers¹². Thus, CDKs are considered critical targets for the development of novel anticancer drugs^{9,10}.

Pyrazolopyrimidine moiety is a common nucleus heterocycle used in the design of different pharmaceutical compounds^{11,12}, with various medicinal applications including antimicrobial, antitumor¹³, antidiabetic, anti-Alzheimer's disease, anti-inflammatory^{14,15}, and antioxidant^{16–18}.

Pyrazolopyrimidine is considered an appealing scaffold for the development of new antitumor agents^{19–24}. This scaffold is considered an adenine bioisostere that retains the essential interactions of ATP at the kinase domain^{25–28}. The pyrazolo[3,4-*d*]pyrimidine bicycle showed great potential in CDK inhibition in drug discovery. It is a purine ring bioisostere with potent growth inhibitory activity^{29,30}, via CDK inhibition as CDK1³¹, CDK2³², and 5-lipoxygenase enzymes³³. They also possess significant and specific pharmacological activity in CDK2/Cyclin A inhibition¹¹. Among the

CONTACT Nasser S. M. Ismail  nasser.saad@fue.edu.eg  Pharmaceutical Chemistry Department, Faculty of Pharmacy, Future University in Egypt (FUE), Cairo, 11835, Egypt

 Supplemental data for this article is available online at <https://doi.org/10.1080/14756366.2022.2086866>

© 2022 The Author(s). Published by Informa UK Limited, trading as Taylor & Francis Group.

This is an Open Access article distributed under the terms of the Creative Commons Attribution-NonCommercial License (<http://creativecommons.org/licenses/by-nc/4.0/>), which permits unrestricted non-commercial use, distribution, and reproduction in any medium, provided the original work is properly cited.

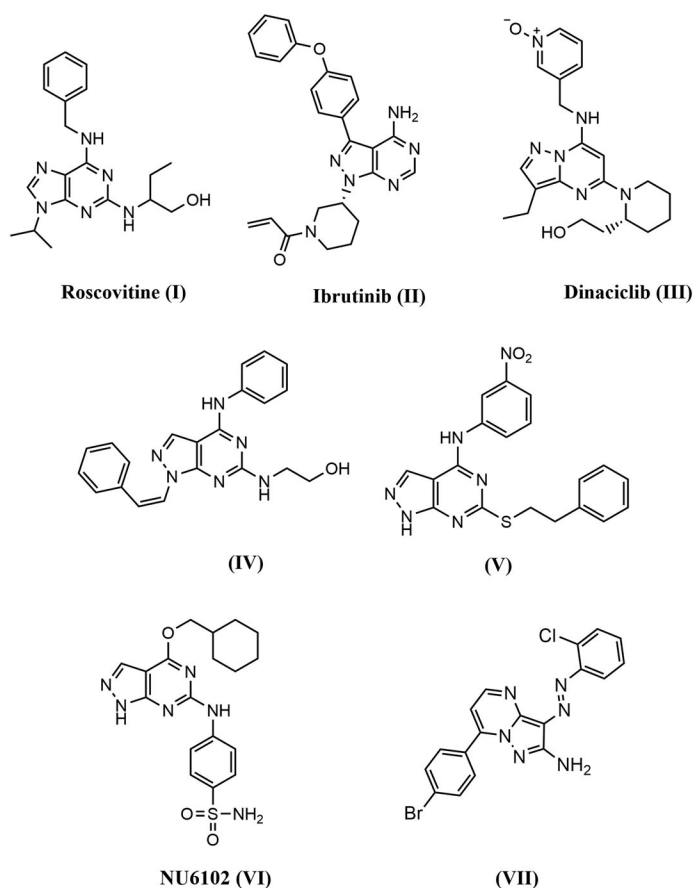


Figure 1. Structures of active drugs containing fused pyrimidine (I) Roscovitine, (II) Ibrutinib, and (III) Dinaciclib, Reported pyrazolo[3,4-*d*]pyrimidines derivatives (IV), (V), and (VI), and Reported pyrazolo[1,5-*d*]pyrimidines derivative (VII) as CDK2 inhibitors.

known drugs of potent CDK2 inhibition are Dinaciclib, Ibrutinib, and Roscovitine^{1,9,12,25,34,35} (Figure 1).

The aim of this research was based on the previously reported work with a rationale for anticancer drug discovery research, to design and synthesise new pyrazolo[3,4-*d*]pyrimidine and its glycosyl amino derivatives as well. In addition to the thioxo-pyrazolo[4,3-*e*][1,2,4]triazolo [1,5-*c*]pyrimidine compounds and the thioglycoside derivatives, based on pyrazolo[3,4-*d*]pyrimidine scaffold to develop novel CDK2 inhibitors^{34,35}. The new derivatives were evaluated for their *in vitro* anti-proliferative activity against three cell lines: breast cancer (MCF-7), hepatocellular carcinoma (HepG-2), and colorectal carcinoma (HCT-116) cell lines. The potential inhibition of the most potent promising compounds on CDK2/Cyclin A was also tested. Also, molecular docking studies were applied to investigate the binding mode of the promising compounds by calculating their binding energies and visualising their orientations with respect to the active site of CDK-2 protein compared to the Roscovitine ligand. The computational results were in agreement with the reported observations.

1.1. Rational design

The design of the new pyrazolo[3,4-*d*]pyrimidine derivatives in compounds 4–6 and pyrazolo[4,3-*e*][1,2,4]triazolo[1,5-*c*]pyrimidin derivatives in compounds 7–15 was based on lead compounds Roscovitine and compound VII optimisation by structural modifications according to their reported binding mode (Figures 2 and 3) where¹².

Purine scaffold was bioisosterically replaced by two different ring systems first: pyrazolo[3,4-*d*]pyrimidine in compounds 4–6 and second: pyrazolo[4,3-*e*][1,2,4]triazolo[1,5-*c*]pyrimidin in compounds 7–15 through the hydrophobic binding with Leu134, Val18, Val64, Ala31, Ala144, Ile10, and Phe80. This is required to place the compound in the ATP adenine region.

The two essential hydrogen bonds in the phosphate binding region with Leu83,1 HBD by –NH of the 6-substituted amino moiety, 1 HBA through N7 in Roscovitine, were replaced by N arylglycyl moiety in all the presented compounds.

The N5 pyrazolopyrimidine substitution by amino group (in compound 4) or N-glycosyl (in compounds 5 and 6) replaced the N butanol at position 2 of Roscovitine.

The pyrazolopyrimidine hydrophobic binding with Ala31, Val18, and Leu134 was maintained as in lead compound and the triazole ring fusion was considered in compounds 7–15 with hydrophobic binding with Val18.

In compounds 7–13, an additional hydrogen bonding by the thio group was achieved as in compound 8 with Asp145. And a hydrogen bond for compound 13 via the acetyloxy moiety with Thr14 was observed.

The hydrophobic binding with Ile10 by the benzyl group in Roscovitine and para bromophenyl group in compound VII was maintained by the isosteric replacement by the para fluorophenyl group in all the new compounds. In addition to the hydrogen binding via the para fluoro group with Lys89 in compounds 8, 9, 11, and 13. As in reported compound VII where it was published that substitution of the phenyl ring with halogen atom is preferable to the un-substituted ring for its cytotoxic effect, with either bromo, fluoro, or chloro group²⁵. While a halogen hydrogen bond formation by compound 11 with Glu8 and compounds 14 and 15 with Asp145 was observed too.

The thioglycoside group at position 2 in compounds 14 and 15 showed also additional Carbon- Hydrogen binding with Glu8.

2. Materials and methods

2.1. Chemistry

5-Amino-1-(4-fluorophenyl)glycyl)-1*H*-pyrazole-4-carbonitrile **2**, was prepared by the reaction of 2-((4-fluorophenyl)amino)acetohydrazide **1** with ethoxymethylene malononitrile in ethanol under reflux. The isolated brown solid **2** was then treated with triethox-yorthoformate in acetic anhydride to afford ethyl-*N*-(4-cyano-1-((4-fluorophenyl)glycyl)-1*H*-pyrazol-5-yl)formimidate **3**. The key starting material pyrazolopyrimidine **4** was obtained by treatment of the formimidate derivative **3** with hydrazine hydrate in ethanol. Subsequent reaction of pyrazolopyrimidine **4** with sugar aldoes namely; D-glucose and D-xylose, in the presence of a catalytic amount of acetic acid, afforded the amino-sugar products **5** and **6** respectively (Scheme 1). The structures of this set of novel amino sugars were confirmed by their spectral and elemental analysis data (see Experimental Section). ¹H NMR spectra of the amino-sugar compounds **5** and **6** showed a signal attributed to H-1 at 5.13 and 5.10 ppm confirming the sp³ hybridisation of its corresponding carbon (C-1) and the cyclic form of the sugar moiety which agrees well with the reported results for such type of compounds following such mode of preparation³⁶.

Adding a carbon disulphide to pyrazolopyrimidine **4** in the presence of potassium hydroxide in ethanol afforded the corresponding triazolomercapto derivative **7**. The ¹H NMR spectra of compound **7** revealed the disappearance of the NH₂ and NH signals and instead another broad singlet at 11.66 ppm for the NH in

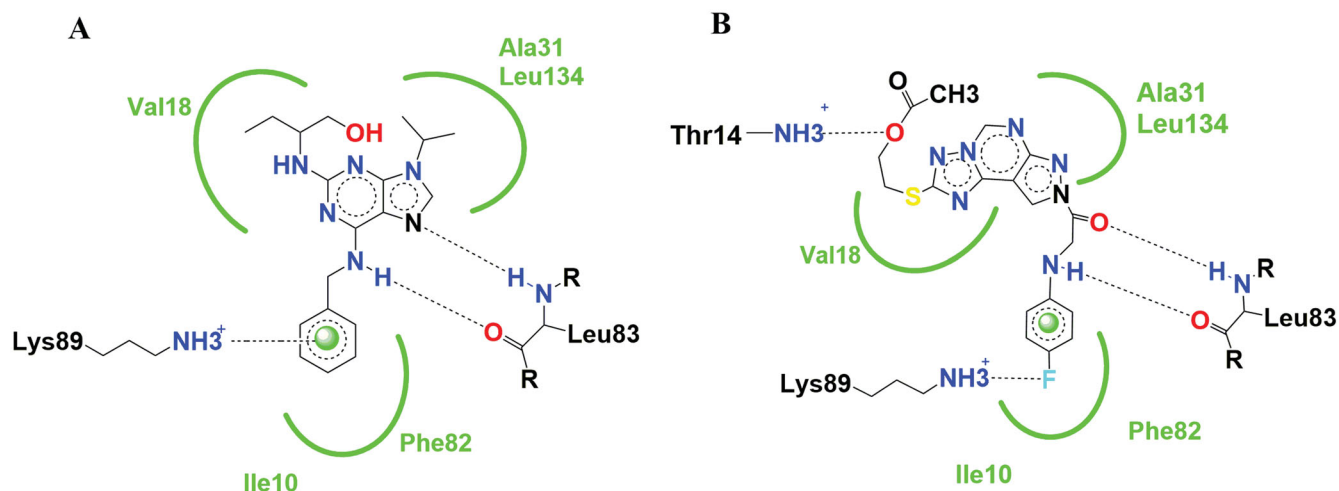


Figure 2. Binding mode schematic illustration of Roscovitine ligand (I) (A) and Newly synthesised pyrazolopyrimidine derivative compound 13 (B) with key amino acids at CDK2 binding site.

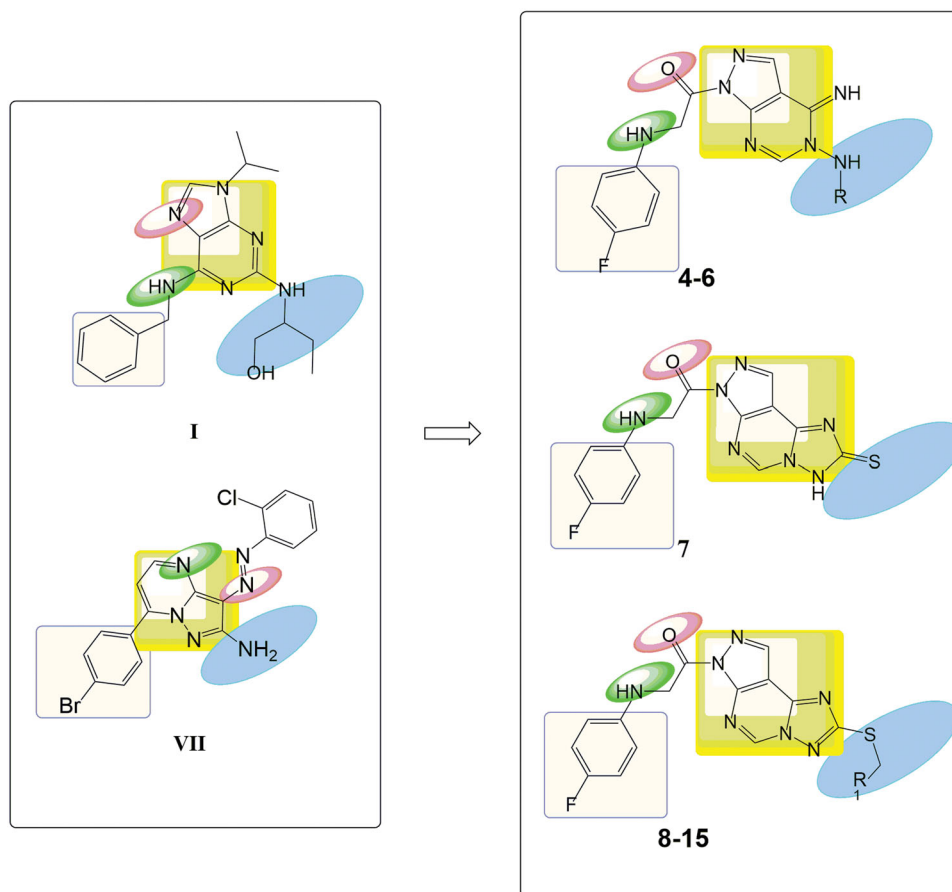
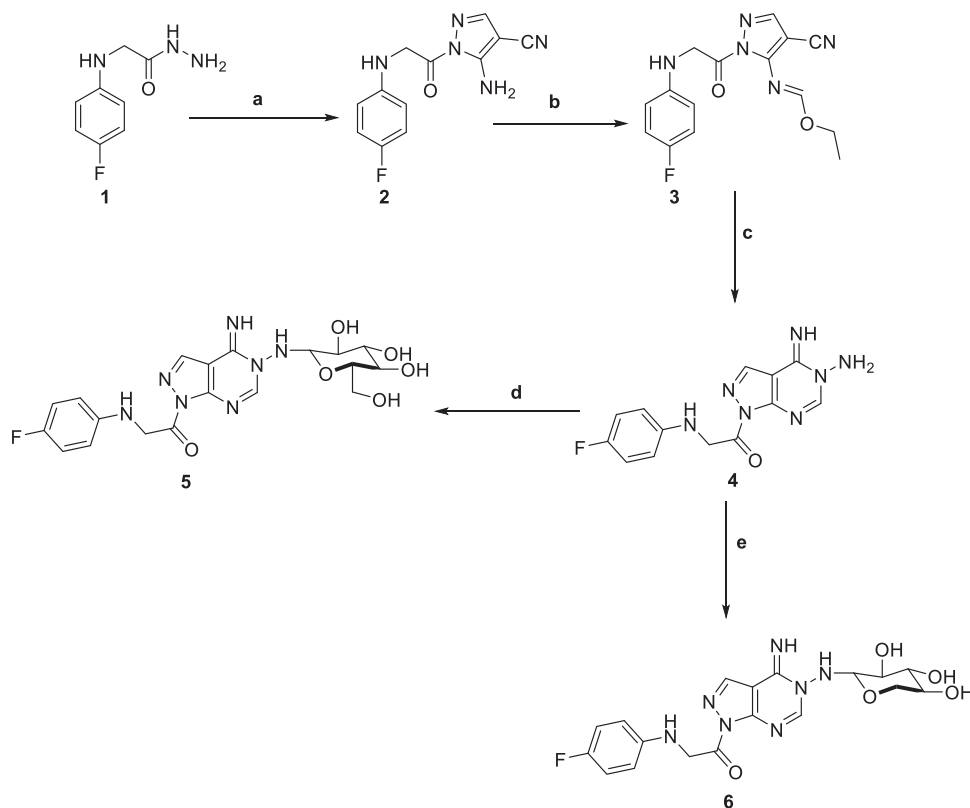


Figure 3. Features' similarities between Roscovitine ligand (I) and reported pyrazolo[1,5-a]pyrimidines derivative (VII) against the newly designed compounds as potent CDK2 inhibitors.

the thione-thiol system appeared. The latter was utilised for the preparation of a series of acyclic nucleoside analogs via reaction with acyclic oxygenated halides. Thus, reaction with chloroacetonitrile, 2-chloro-1,1-dimethoxyethane, 2-chloropropane-1,2-diol, and 2-chloroethan-2-ol by stirring or by reflux in ethanol afforded the thioderivatives **8–10** and **12**, respectively in good yields. In addition, the hydroxyl compounds **10** and **12** were acetylated with acetic anhydride to yield the corresponding *O*-acetylated acyclic analogs **11** and **13**, respectively (Scheme 2). The ^1H NMR spectra

of the resulted acetylated derivatives showed the signals of the acetyl-methyl groups in addition to the disappearance of the hydroxyl signals which was also confirmed by their IR spectra. The latter showed the carbonyl bands of the ester groups and the disappearance of the characteristic bands of the hydroxyl groups (see Experimental Section).

The reaction of triazolo pyrazolo pyridine derivatives **7** with two acetylated glycosyl halides, tetra-*O*-acetyl- α -D-gluco- and galactopyranosyl bromide, afforded the thioglycoside derivatives **14**



Scheme 1. Reagents and conditions; (a) 2-(ethoxymethylene)-malononitrile, EtOH, reflux, 6 h. (b) triethyl orthoformate, acetic anhydride, reflux, 6 h. (c) hydrazine hydrate, EtOH, reflux, 6 h. (d) D-Glucose, EtOH, glacial acetic acid, reflux, 3 h. (e) D-Xylose, EtOH, glacial acetic acid, reflux, 3 h.

and **15** as nucleoside analogs (Scheme 3). The ^1H NMR of compound **14** revealed an increase in the integration of the aliphatic region at 2.23–5.76 ppm, while the ^{13}C NMR spectrum showed the characteristic signals for the five carbons of C=O groups at δ 165 and 175 ppm.

3. Results and discussion

3.1. *In vitro* anti-proliferative activity

All the synthesised compounds were evaluated for their *in vitro* anti-proliferative activities using MTT assay^{37,38}, against three cell lines named: breast cancer (MCF-7), hepatocellular carcinoma (HepG-2), and colorectal carcinoma (HCT-116). Results were compared to reference Sorafenib (Table 1). Most of the compounds **8**, **9**, **10**, **11**, **13**, **14**, and **15** showed superior cytotoxic activities against MCF-7 with IC_{50} range (7–95 nM). While compounds **6**, **8**, **9**, **11**, **13**, **14**, and **15** showed potent activity against HCT-116 with IC_{50} range (6–93 nM) compared to the reference (IC_{50} : 144 and 176 nM, respectively). Only compounds **8**, **14**, and **15** showed potent activity against HepG-2 with IC_{50} values of (8, 7, 7 nM, respectively) compared to the reference (IC_{50} : 19 nM). Compounds **14** and **15** showed the most potent cytotoxic activities against the three cell lines and compound **13** showed moderate HepG-2 activity with IC_{50} 74 nM and superior activity against both MCF-7 and HCT-116 with IC_{50} values of 55 and 9 nM, respectively (Figure 4).

3.2. CDK2/cyclin A2 inhibitory activity

All the synthesised compounds **4**, **5**, **6**, **7**, **8**, **9**, **10**, **11**, **12**, **13**, **14**, and **15** were tested for their *in vitro* CDK2/cyclin A2 assays using

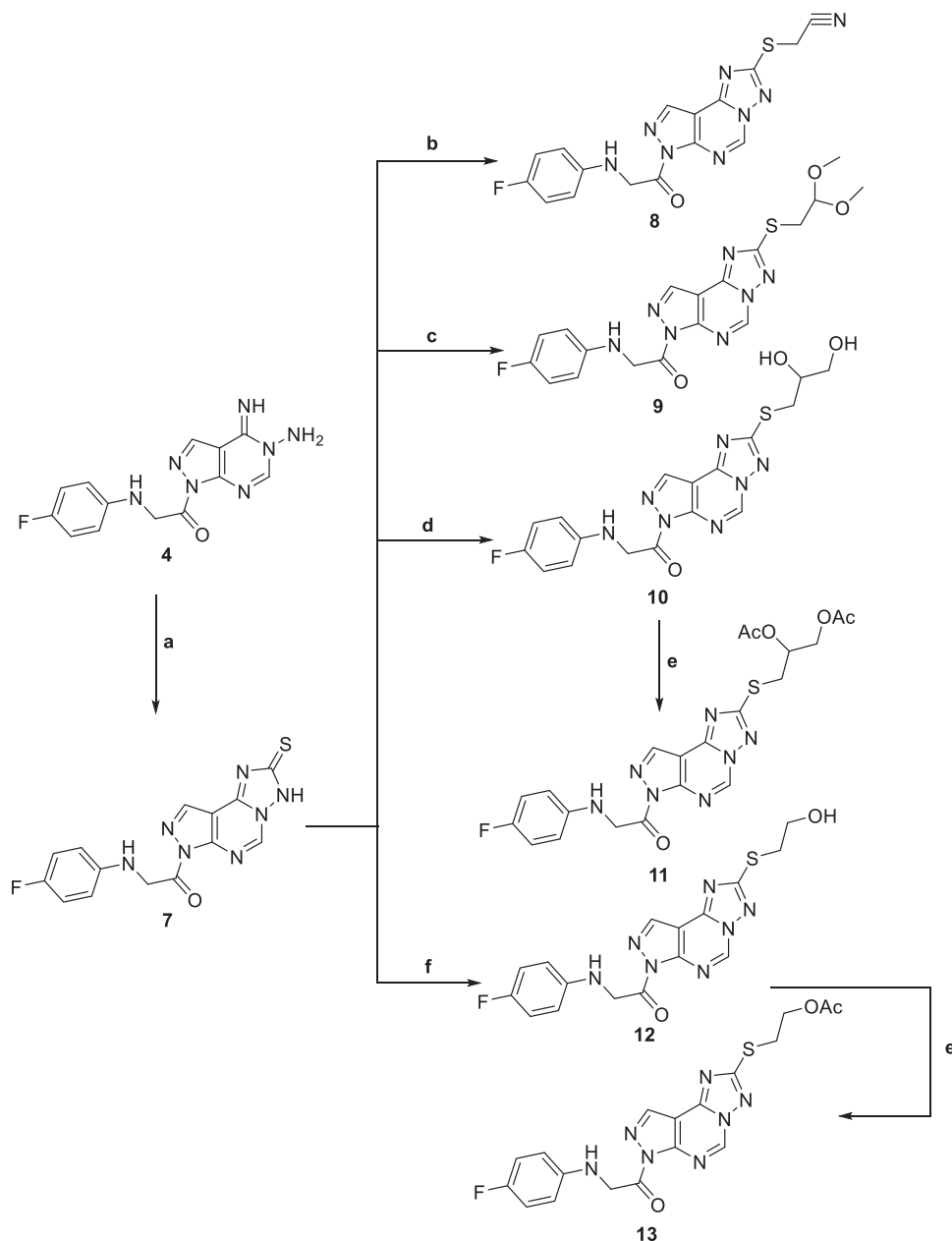
Promega Kinase-Glo Plus luminescence kinase assay³⁹. The assay depends on kinase reaction and ADP measurement, ADP is first transferred to ATP and then converted to light. The produced luminescent signal is directly proportional to the amount of ATP and inversely proportional to the kinase activity. The results of the enzymatic inhibitory activity of the tested compounds against CDK2/cyclin A2 were presented in Table 2. All the tested compounds showed a good inhibitory effect with IC_{50} values ranging from 0.061 ± 0.003 to $2.050 \pm 0.05 \mu\text{M}$ compared to Sorafenib IC_{50} : $0.184 \pm 0.01 \mu\text{M}$ and Dinaciclib IC_{50} : 0.029 ± 0.002 . Results revealed that compounds **15**, **11**, **14**, and **13** showed the most powerful inhibitory activity with IC_{50} values of 0.061 ± 0.003 , 0.089 ± 0.005 , 0.118 ± 0.007 , and $0.13 \pm 0.007 \mu\text{M}$, respectively, compared to control drug Sorafenib and/or Dinaciclib. Where compound **15** showed the superior activity (Figure 5).

3.3. *In vitro* cytotoxicity against normal cells WI-38

The cytotoxic effect of the most active compound **15** against WI-38 normal lung cells was *in vitro* assessed (Table 3) against Staurosporine as a reference standard. Compound **15** showed low cytotoxicity against normal cells compared to the reference standard with IC_{50} values of 69.60 ± 2.47 and $57.57 \pm 1.42 \mu\text{M}$ for the most active compound **15** and reference standard, respectively. This data indicated that the synthesised compounds, more specifically that compound **15** exhibit low cytotoxicity against normal cells than cancer cell lines.

3.4. Flow cytometry cell cycle analysis

Compound **15** showed the most potent enzymatic inhibitory activity against CDK2/cyclin A2 and potent anti-proliferative



Scheme 2. Reagents and condition; (a) CS_2 , KOH, EtOH, reflux, 6 h. (b) Chloroacetonitrile, K_2CO_3 , DMF, 25°C , 8 h. (c) Chloroacetaldehyde dimethyl acetal, K_2CO_3 , DMF, 25°C , 8 h. (d) 2-chloro-1,2-propanediol, KOH, EtOH, reflux, 3 h. (e) Acetic anhydride, pyridine, reflux, 2 h. (f) 2-chloroethanol, KOH, EtOH, reflux, 3 h.

activity against the three selected cancer cell lines. Furthermore, compound **15** was selected for flow cytometry assay to evaluate cell cycle analysis against HCT-116 cells. The cell cycle analysis is used to investigate the mechanism of action of the new compounds⁴⁰. Table 4 presents the results showing Pre-G1 and cell growth arrest in the S phase. Results were compared to normal control cells, in Dip Pre-G1 with an increase from 1.85 to 32.73% for compound **15** (Figure 6).

3.5. Flow cytometric analysis of apoptosis

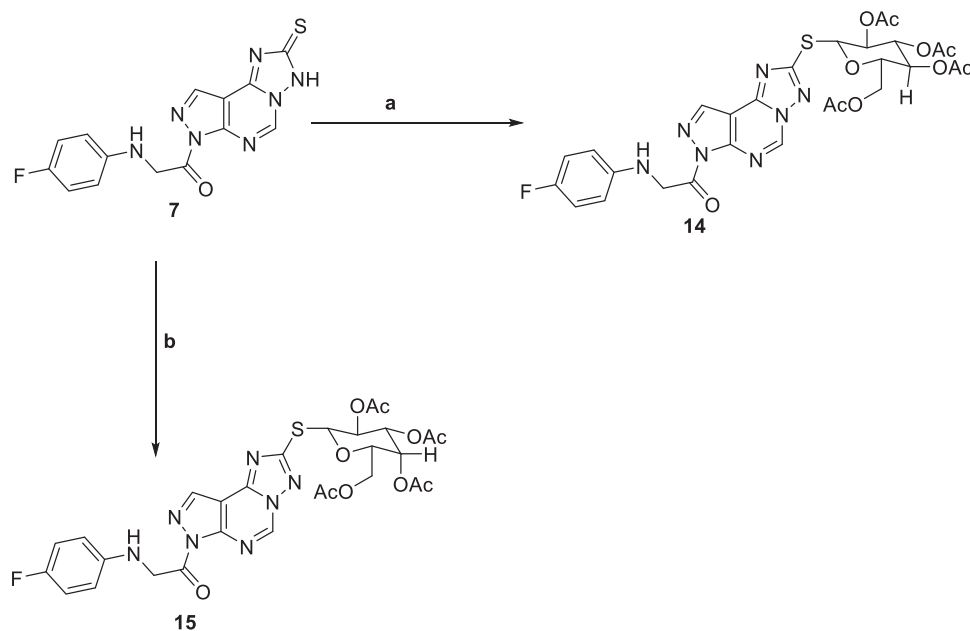
Flow cytometric analysis of apoptosis was performed on compound **15** to determine the potentiality of apoptosis induction against the HCT-116 cell line⁴¹.

Table 5 and Figure 7 showed that compound **15** induced apoptosis by 32.73% (9.26 and 19.12 at early and late apoptosis,

respectively), which was 17.69 times more than the standard control (1.85%).

3.6. Molecular docking

A molecular docking study using the C-Docker protocol in Discovery Studio 4.0 Software was performed on all the synthesised compounds. The compounds were prepared and then docked into the binding site of the CDK2 enzyme. An analysis study was applied to determine the binding modes of the designed compounds and to interpret the biological results. Hence, more explanation about the binding poses and interactions with the key amino acids in the binding site was noticed. X-ray crystallographic structure of CDK2 being complexed with Roscovitine (PDB ID: 2A4L) was downloaded from Protein Data Bank^{9,12}. It was known from the previous literature that there are two essential



Scheme 3. Reagents and conditions; (a) 2,3,4,6-Tetra-O-acetyl-D-glucopyranosylbromide, KOH, acetone, 25 °C, 6 h. (b) 2,3,4,6-Tetra-O-acetyl-D-galactopyranosylbromide, KOH, acetone, 25 °C, 6 h.

Table 1. The *In vitro* anti-proliferative activity of the synthesised compounds against human cell lines.

Compound ID	<i>In vitro</i> IC ₅₀ (nM) Mean ± SD		
	MCF-7	HepG-2	HCT-116
Sorafenib	144 ± 0.47	19 ± 0.29	176 ± 0.69
4	150 ± 1.5	603 ± 1.9	521 ± 0.67
5	663 ± 1.4	690 ± 0.48	503 ± 0.97
6	621 ± 2.7	98 ± 0.78	93 ± 0.35
7	937 ± 0.93	63 ± 0.11	926 ± 1.6
8	72 ± 0.53	8 ± 0.34	52 ± 0.44
9	60 ± 0.49	690 ± 1.6	71 ± 0.46
10	95 ± 1.9	987 ± 2.0	664 ± 0.93
11	63 ± 1.1	49 ± 0.17	7 ± 0.61
12	613 ± 0.33	928 ± 0.97	587 ± 0.88
13	55 ± 0.43	74 ± 1.1	9 ± 0.06
14	7 ± 0.17	7 ± 0.43	6 ± 0.17
15	8 ± 0.29	7 ± 0.3	10 ± 0.27

hydrogen bonds with Leu83 at the active site besides hydrophobic interactions^{9,12}. Validation was confirmed by re-docking of Roscovitine in the active site of CDK2 with RMSD value = 0.5 Å. Superimposition of co-crystallised ligand and ligand after docking indicates the perfect superimposition at the binding site (Figure 8). The best pose out of ten for each compound was selected showing maximum similarity to the binding mode compared to the ligand. The presented docking study showed comparable binding modes to the lead compound for the docked molecules.

The interaction energy with the essential amino acids of the most biologically active synthesised compounds at the active site is demonstrated in Figure 9(A,B). Results showed comparable binding interaction energy to the lead compound Roscovitine ($E = -55.75$ kcal/mol), ranging from 60.89 to 50.85 kcal/mol). Compound 15 revealed a binding score = -59.85 kcal/mol with a similar binding mode.

All the docked molecules revealed a hydrogen bond with Leu83. Most of the compounds formed 1 HBD through -NH of glycylyl group where binding distance range was observed to be within (2.02–2.10 Å) and 1 HBA through the oxygen atom of the carbonyl group of the glycylyl moiety with a binding distance range

of (2.20–2.74 Å) (Figure 9(A,B)). Compounds 4,5,6,10, and 12 showed different binding modes with either two hydrogen bonds with Leu83 as in compounds 4 and 6, or only one hydrogen bond as in compounds 5, 10, and 12. The sugar moiety in compounds 5 and 6 was responsible for the HBD interaction with Leu83 (Supplementary Material).

All the tested compounds showed binding via the parafluorophenyl group except compounds 4, 5, 7, 8, and 10. Either by a hydrogen bond with Lys89 as in compounds 9, 11, and 13 or by halogen hydrogen binding with Asp145 as in compounds 14 and 15 or extra binding with Glu81 as in compound 11. Compounds 6 and 12 undergo one halogen hydrogen bond with Glu81 and His84 via the parafluoro group, respectively. Compounds 7 and 11 showed only 1 HBD with Leu83 (compound 11 showed better interaction energy after docking than compound 7). Also, compound 11 (the diacetoxo derivative) and compound 13 (the monoacetoxo derivative) showed an extra hydrogen bond with Thr14 via the acetyloxy group. Compounds 14 and 15 showed additional HBD with Glu81 via the -NH group of the glycylyl moiety.

Also, the docked compounds showed comparable hydrophobic binding to lead compounds with Leu134, Val18, Val64, Ala31, Ala144, Ile10, and Phe80.

3.7. *In silico* predictive ADMET study

The design and development of novel drug molecules need early investigation of pharmacokinetic properties including absorption, distribution, metabolism, and excretion (ADME), at a stage where access to the physical samples is limited⁴¹. It was observed that the limited pharmacokinetic or toxicity profile of new drug-like molecules had a great influence on the low percentage of the drugs that could reach to clinical development stage to be ready to reach the market⁴².

Several ways for *in silico* predictive ADMET studies have been developed. Including web-based platforms, such as ADMETlab, Pro Tox-II, and SwissADME to predict ADMET properties⁴².

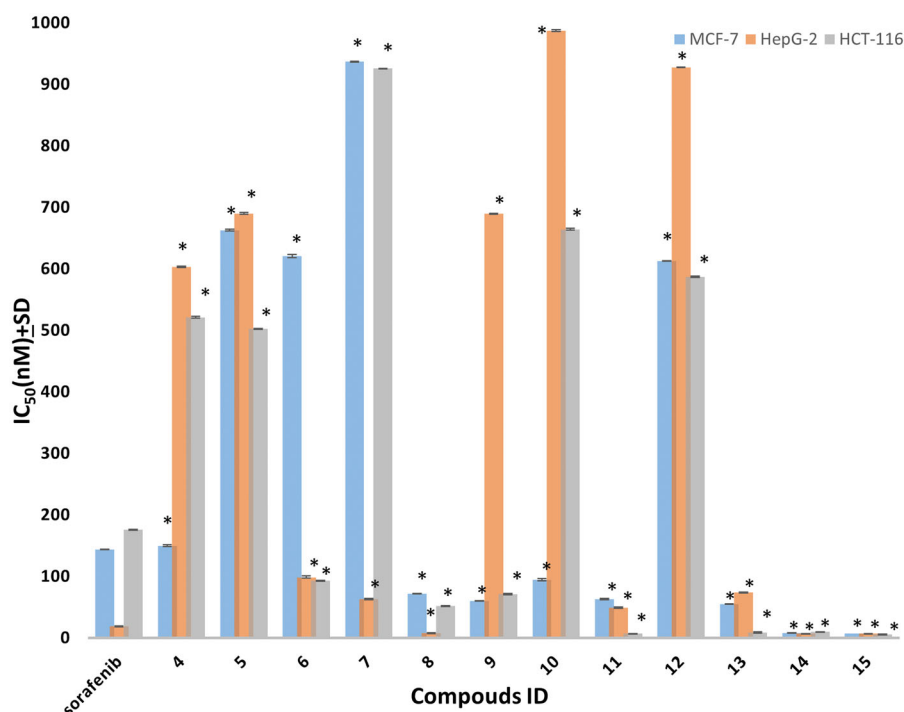


Figure 4. The IC_{50} of tested compounds against MCF-7, HepG-2, and HCT-116 cancer cell lines. Data expressed as mean \pm SD from three independent repeats ($n = 3$). *Significant from sorafenib at $p < 0.05$.

Table 2. CDK2/cyclin A2 inhibitory activity results of all synthesised compounds.

Compound ID	CDK2/cyclinA2 IC_{50} (μ M) \pm SD
Sorafenib	0.184 \pm 0.01
Dinaciclib	0.029 \pm 0.002
4	1.342 \pm 0.021*, #
5	2.050 \pm 0.05*, #
6	0.559 \pm 0.013*, #
7	0.274 \pm 0.005*, #
8	1.064 \pm 0.059*, #
9	0.881 \pm 0.049*, #
10	0.506 \pm 0.011*, #
11	0.089 \pm 0.005*
12	0.961 \pm 0.019*, #
13	0.13 \pm 0.007#
14	0.118 \pm 0.007*, #
15	0.061 \pm 0.003*

*Significant from sorafenib at $p < 0.05$.

Significant from dinaciclib at $p < 0.05$.

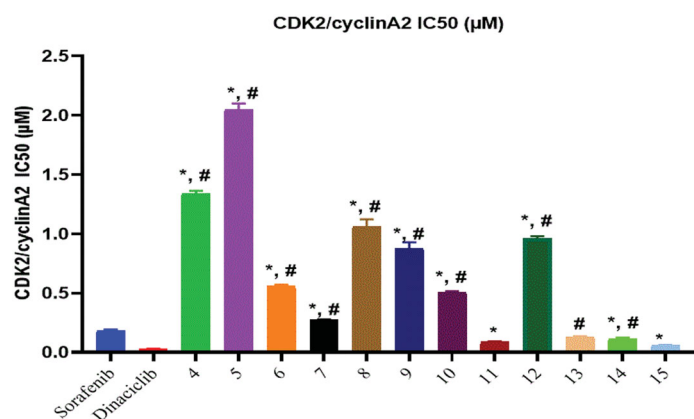


Figure 5. Inhibitory activity of most potent compounds on CDK/Cyclin A2. *Significant from sorafenib at $P < 0.05$, # Significant from dinaciclib at $P < 0.05$.

Here in this research ADMET study was performed mainly using Discovery Studio 4.0 Software for all the synthesised compounds.

Table 3. The *In vitro* cytotoxicity of the most active compound 15 and Staurosporine against normal lung cells (WI-38).

Compound ID	<i>In vitro</i> IC_{50} (μ M) as Mean \pm SD
15	Normal cell WI-38 69.60 \pm 2.47
Staurosporine	57.57 \pm 1.42

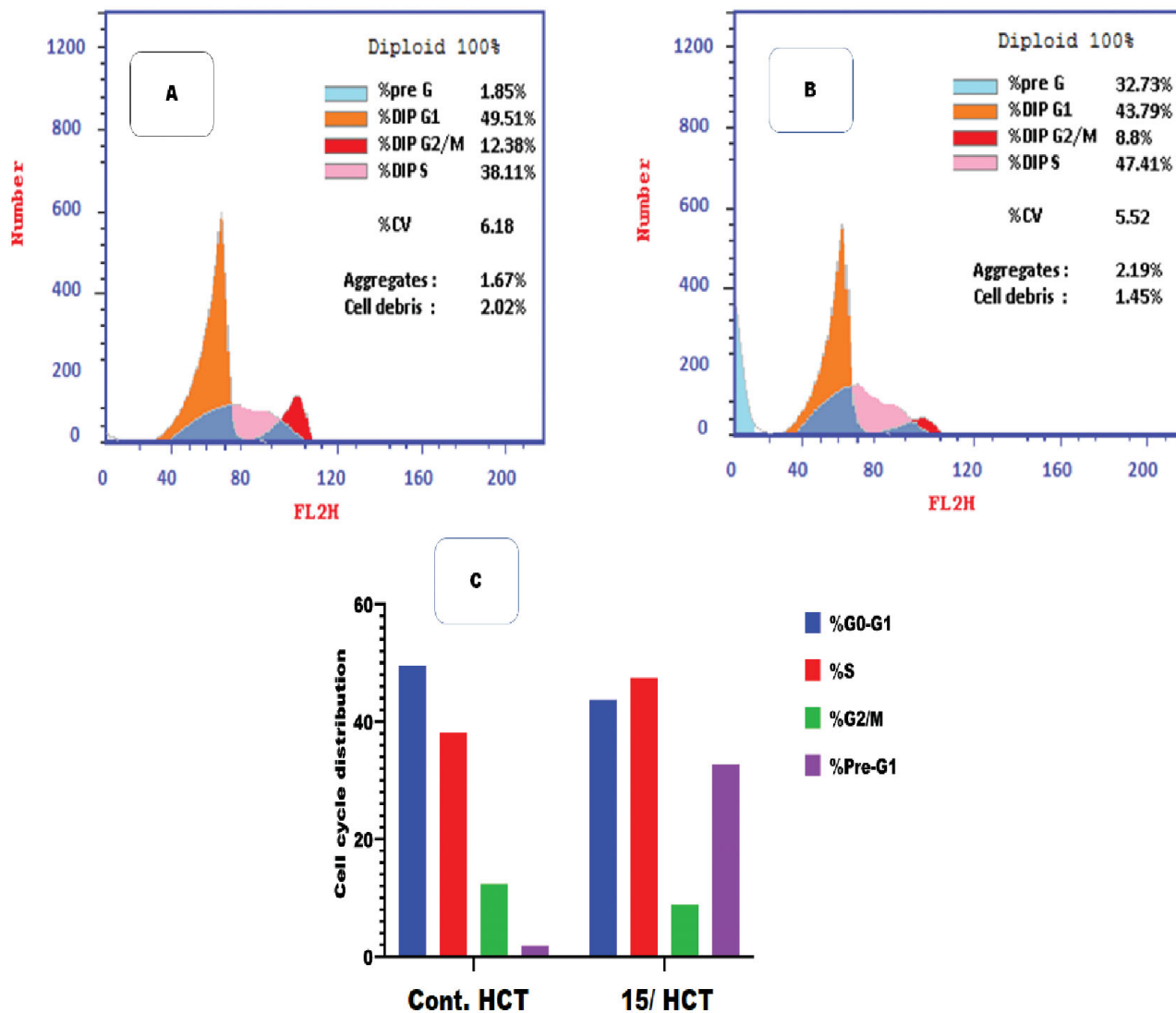
Also, the ADMETlab web tool was used to confirm results on the highly potent molecules with promising molecular docking results only to assure the early investigation of their pharmacokinetic properties and compare to Roscovitine as a control drug⁴³.

The ADMET study using Discovery Studio 4.0 Software is mainly concerned with the chemical structure of the molecule, it includes several parameters calculation; Blood Brain Barrier Level, Absorption level, Atom-based Log P98 (A LogP 98), 2D polar surface area (ADMET 2D PSA), Cytochrome P450 2D6 (CYP2D6), Hepatotoxicity Probability, Aqueous solubility level, and Plasma protein binding logarithmic level (PPB Level).

Results shown in Table 6 reveals that all the compounds had BBB level of 3 and 4. So, they are not able to pass the blood-brain barrier. Most of the compounds had absorption levels = 0 or 1, thus estimated to have good to moderate human intestinal absorption, whilst only compounds 4, 5, 14, and 15 showed low absorption. All the compounds showed ADME aqueous solubility levels between 2 and 3 which indicates good aqueous solubility except compounds 7, 8, and 9 which showed low aqueous solubility. The key property (PSA) was linked to drug bioavailability. Therefore, molecules that are passively absorbed and PSA < 140 are thought to have lower bioavailability. Most of the synthesised compounds were predicted to present good passive oral absorption except compounds 4, 5, 14, and 15 which showed good bioavailability results with a PSA range of 168.67–199.705. Compound 4 showed no hepatotoxicity. Also, all the compounds are considered non-inhibitors to Cytochrome P450 2D6 (CYP2D6) and are

Table 4. Flow cytometric analysis for cell cycle distribution of compound 15 on HCT-116 cells.

	Results DNA content				Comment
	%G0-G1	%S	%G2/M	%Pre-G1	
Control/HCT-116	49.51	38.11	12.38	1.85	
Compound 15/HCT-116	43.79	47.41	8.8	32.73	Cell growth arrest at S phase

**Figure 6.** Flow cytometric analysis for cell cycle distribution. (A) Control HCT, (B) Compound 15, and (C) graphical representation for cell cycle distribution analysis among differently treated cells.**Table 5.** Effect of compound 15 on apoptosis in HCT-116 cells.

	Apoptosis			Necrosis
	Total	Early	Late	
Control HCT-116	1.85	0.34	0.28	1.23
Compound 15/HCT-116	32.73	9.26	19.12	4.35

poorly bounded to plasma proteins except compounds **2** and **3**. (Table 6).

Also, the ADMETlab web tool was used to predict the pharmacokinetics of the most promising synthesised compounds. The results were compared to the control drug (Roscovitine)⁴³.

ADMETlab was used to determine the Physicochemical Properties using different descriptors (logS, logD, and logP), Absorption: CaCO₃ Permeability (CaCO₂) (human colon carcinoma

cell line Caco-2), Human Intestinal Absorption (HIA), P-gp inhibitor/substrate (Pgp), 20% bioavailability (as F20%), and 30% bioavailability (as F30%), Distribution: Blood Brain Barrier (BBB), Plasma Protein Binding (PPB) and Volume of Distribution (VD) and Excretion: as both Half-Life (T_{1/2}) and Clearance (CL). Some properties were expressed numerically as CaCO₂, VD, PPB, CL, and T_{1/2}, while others were expressed categorically including the rest of the pharmacokinetic parameters⁴².

Also, Toxicity profiles, such as H-HT (Human Hepatotoxicity) and CYP2D6 were predicted using ADMETlab.

Lipinski's rule of five is an essential tool for rational drug design. The low permeability or poor absorption for tested compounds was related to a disturbance in one of Lipinski's rules of five⁴². Molecular weight, LogP, and the number of hydrogen bond acceptors (NHBA) should lie within the values of <500, 3, and 10,

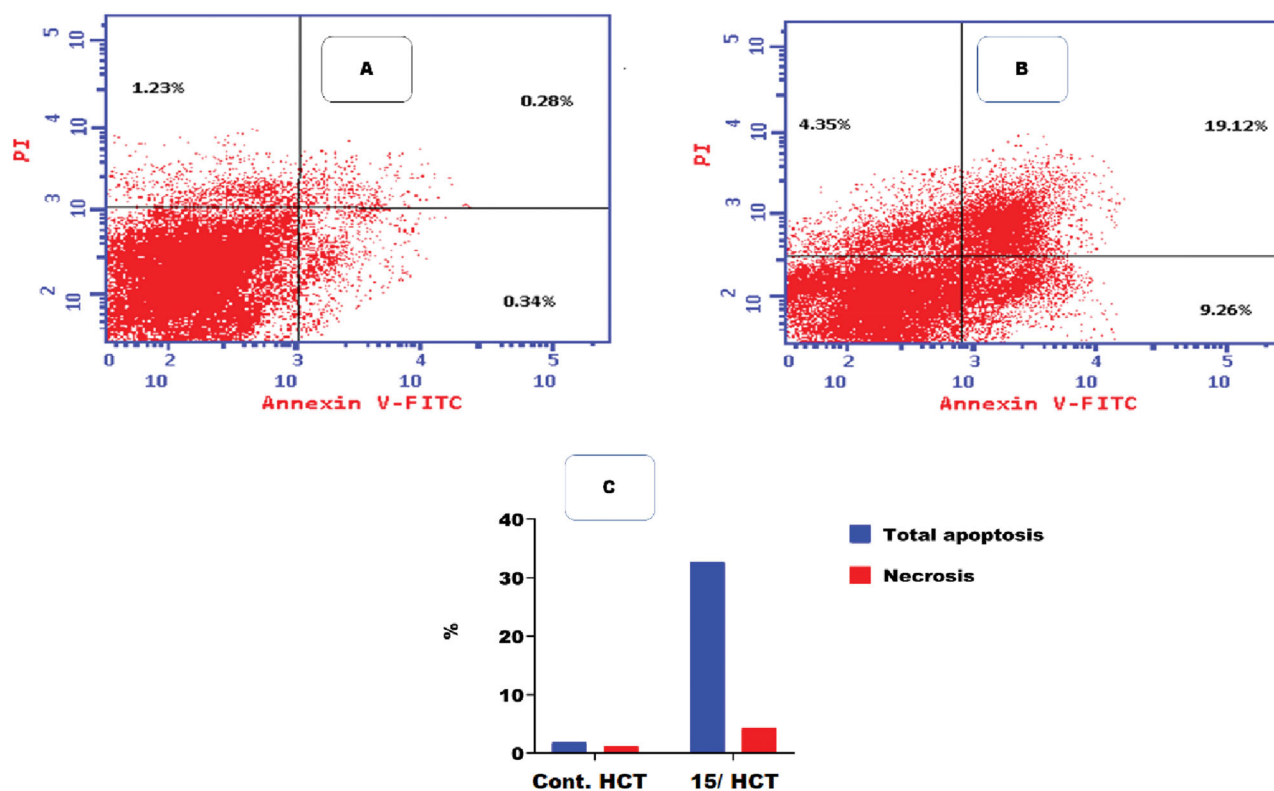


Figure 7. Flow cytometric analysis of apoptosis among treated cells. (A) Control HCT, (B) Compound 15, and (C) Graphical illustration of apoptosis % among differently treated cells.

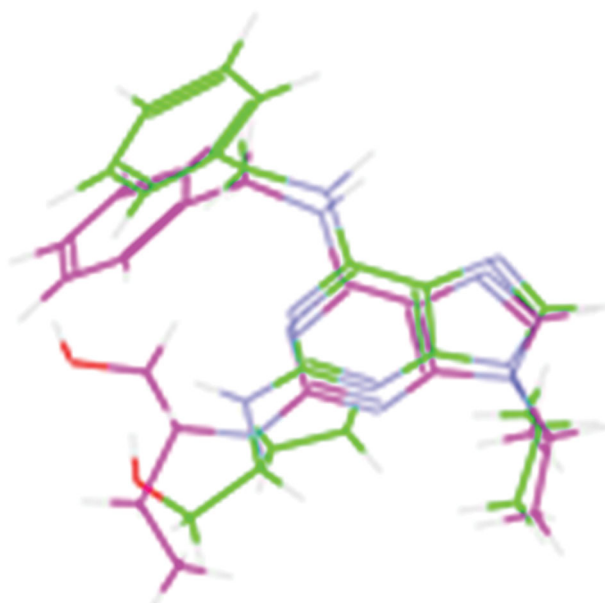


Figure 8. The superimposition 3D diagram of co-crystallised (green colour) and ligand after docking (purple colour) at the active site.

respectively. Hereby, all the compounds except compound **8** had NHBA of 10 or more. Compounds **11**, **14**, and **15** showed low aqueous solubility and poor absorption. Where it was observed from log *S* results that all the tested drugs showed non-aqueous solubility values in the range of -5.401 to -4.731 compared to the control drug (optimal: $-4-0.5$ log mol/L). While, the log *P* results showed optimal lipophilicity values (Optimal: $0 < \text{Log} P < 3$) (Table 7).

Molecules having similar molecular mass showed similarities in Topological Polar Surface Area (TPSA, %Abs). Where molecules with a TPSA of 140 \AA and more showed poor absorption ($<10\%$ fractional absorption) as in compounds **11**, **14**, and **15**, while those with a TPSA of 60 \AA showed good absorption ($>90\%$)⁴² (Table 7).

3.7.1. Pharmacokinetics properties

3.7.1.1. Absorption. To evaluate the absorption property, CaCO₂ Permeability (Caco-2-Permeability), P-glycoprotein (P-gp), substrate or inhibitor (P-gpinh/P-gpsub), Human intestinal absorption (HIA), 20% bioavailability (F20), and 30% bioavailability (F30) were predicted and results were presented in Table 8.

It is found that the values of Caco-2-Permeability were in the range from -4.647 to -5.49 cm/s, suggesting to have optimal permeability except for compounds **14** and **15** which showed a -5.49 cm/s result. (optimal permeability more than -5.15 cm/s)

The predicted HIA data of the tested compounds are represented categorically as 1, where Category 1: HIA+ (HIA $\geq 30\%$); Category 0: HIA- (HIA $< 30\%$). The output value indicated a high HIA probability for the tested compounds except for compounds **14**, **15**, and the control drug. Most of the compounds showed good bioavailability, Compounds **14** and **15** showed 20–30% bioavailability.

3.7.1.2. Distribution. To study the distribution of drug candidates some parameters were considered as Plasma Protein Binding (PPB), Blood Brain Barrier (BBB) permeability, and Volume of distribution (VD) (Table 7). The PPB was predicted to exceed 90% to bind significantly to blood proteins compared to the control drug. While BBB results showed that all the tested compounds have no BBB penetration effect except compounds **14** and **15**.

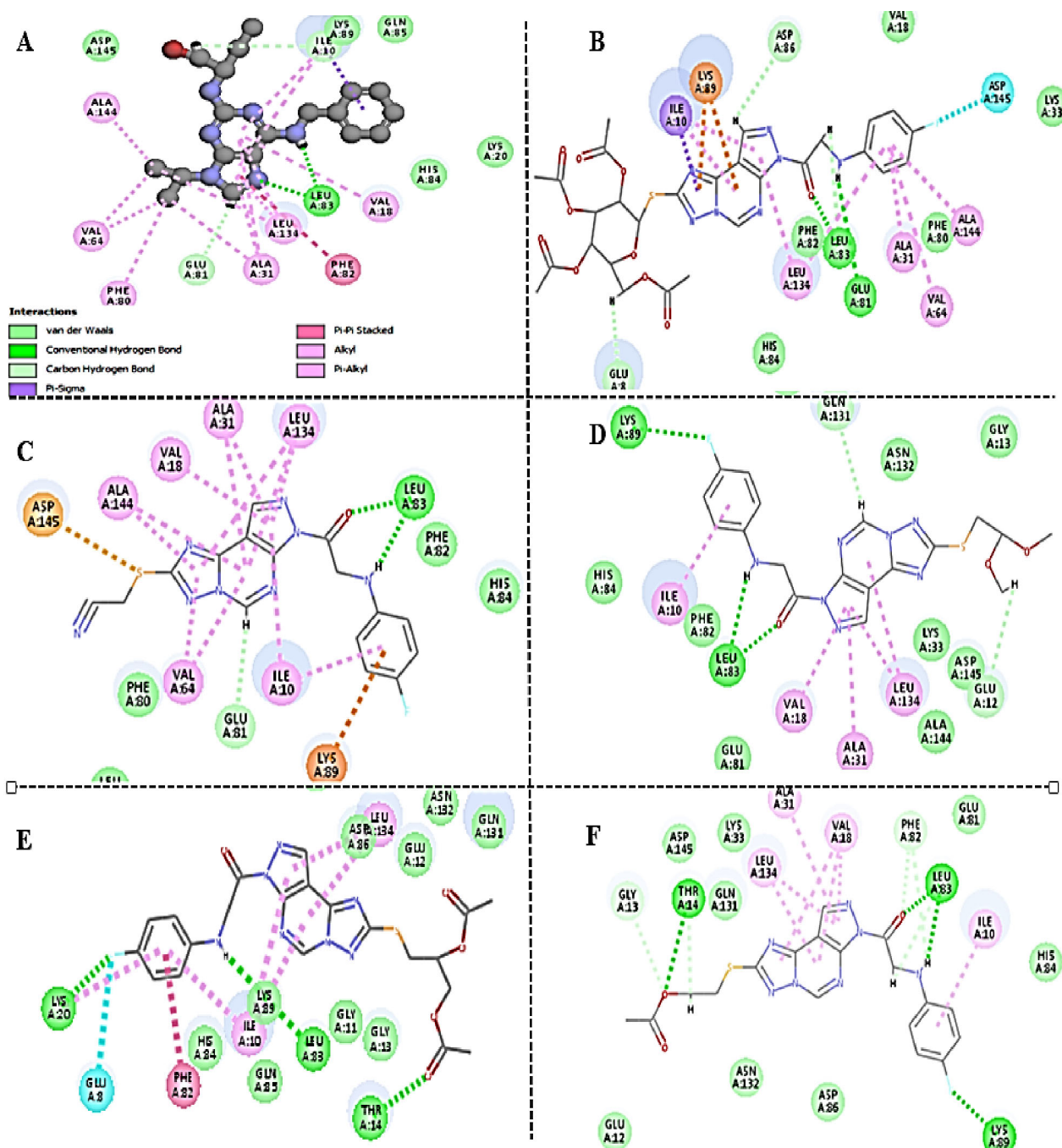


Figure 9. (A) The proposed binding mode of the most promising compounds after docking compared to lead compound: Roscovitine (A), compound 15 (B), compound 8 (C), compound 9 (D), compound 11 (E), and compound 13 (F) within the active site of CDK2 resulting from docking. (B) The proposed 3D binding mode diagram of the most promising compounds after docking compared to lead compound: Roscovitine (A), compound 15 (B), compound 8 (C), compound 9 (D), compound 11 (E), and compound 13 (F) within the active site of CDK2 resulting from docking.

The volume of distribution (VD) in L/Kg was predicted to be optimal when it lies in the range of: 0.04–20 L/kg. So, all compounds showed good VD with moderate clearance results (except compounds **11**, **14**, and **15** with low clearance results). The hydrophobic character of the compounds was contributed to good values of VD in tissues which confirmed absorption and distribution parameters. Also, all the tested compounds were non-inhibitors to CYP2D6 and showed no hepatotoxicity.

The most potent anti-proliferative compound **15**, as compared to the control drug Roscovitine. Where related pharmacokinetic parameters showed the probability of the same physicochemical characteristics and related behaviour inside the human body with

similar biological effects. Figure 10 showed related pharmacokinetic properties showing differences mainly in the number of nHD due to differences in their chemical structure.

3.8. Structure–activity relationship

The structure–activity relationship of the novel compounds was studied based on their biological evaluation in addition to the molecular studies results. Where in the pyrazolo[3,4-*d*]pyrimidine scaffold in compounds (**4**–**6**), it was observed that the N5 pyrazolopyrimidine D-Xylose substitution showed potent activity against

Table 6. *In silico* ADMET predictions of the newly synthesised compounds using Discovery Studio.

Name	BBB LEVEL	ADMET Absorption level	ADMET A log P98	ADMET PSA 2D	Cytochrome P450 2D6 (CYP2D6) (non-inhibitor)	Hepato-toxicity	ADMET Aq Solubility level	PPB-Level (poorly bounded)
2	3 (low)	0 (good)	1.051	96.195	-5.658	true	3 (good)	0.007
3	3 (low)	0 (good)	2.095	89.908	-3.936	true	3 (good)	2.494
4	4	3 (v. low)	0.143	168.67	-6.932	false(non-toxic)	3 (good)	-6.288
5	4	3 (v. low)	-0.648	189.486	-2.309	true	3 (good)	-11.215
6	3 (low)	0 (good)	0.913	111.023	-4.481	true	3 (good)	-2.893
7	3 (low)	0 (good)	2.291	85.529	-5.219	true	2 (low)	-1.158
8	4	0 (good)	2.275	108.786	-3.780	true	2 (low)	-2.374
9	3 (low)	0 (good)	2.482	103.711	-3.424	true	2 (low)	-2.444
10	4	0 (good)	1.494	127.482	-4.059	true	3 (good)	-7.124
11	4	1 (Moderate)	2.253	138.313	-5.385	true	3 (good)	-4.920
12	3 (low)	0 (good)	2.005	106.667	-3.563	true	3 (good)	-3.724
13	4	0 (good)	2.384	112.082	-3.468	true	3 (good)	-3.661
14	4	3 (v. low)	1.906	199.705	-6.713	true	3 (good)	-7.699
15	4	3 (v. low)	1.906	199.705	-6.713	true	3 (good)	-7.699

Table 7. Physicochemical properties predictions of the most potent promising compounds using ADMETlab.

Name	Mol wt	nHBAs	nHBDs	Log P	Log S	Log D	TPSA
8	382.08	9	1	2.278	-5.401	2.353	113.79
9	431.12	10	1	2.576	-4.731	2.65	108.46
11	501.12	12	1	2.984	-4.846	2.454	142.6
13	429.1	10	1	2.928	-5.276	2.61	116.3
14	637.16	17	1	2.66	-5.104	1.999	204.43
15	637.16	17	1	2.66	-5.104	1.999	204.43
Roscovitine	354.22	7	3	2.421	-2.807	-2.643	94.35

The bold values express values of 140 Å or more showing poor absorption of compounds 11, 14 and 15.

HCT-116 cell lines and moderate activity against HepG-2 cell lines compared to D-Glucose derivative or the unsubstituted derivative that was inactive against the three cell lines (Figure 11).

While after the triazole ring fusion in pyrazolo[4,3-*e*][1,2,4]triazolo[1,5-*c*]pyrimidin scaffold (**7–15**), the *in vitro* anti-proliferative activity results revealed that compounds **14** and **15** showed the best cytotoxic results that might be related to the thioglycosidic substitution on triazole ring. The thioalkyl substituents as the monoacetoxy alkyl group in compound **13** and diacetoxy alkyl in **11** showed the most potent cytotoxic results against HCT-116 cell lines with good activity against MCF-7 and moderate activity against HepG-2 cell lines compared to other derivatives. While the dihydroxy alkyl derivative **10** showed only potent activity against MCF-7 cell lines. The acetonitrile derivative **8** showed potent activity against HepG-2 cell lines, compared to the dimethoxy alkyl substitution in compound **9** with no activity against HepG-2 cell lines. The monohydroxy alkyl derivative **12** was inactive against the three cell lines. While the thioxo derivative **7** showed only moderate activity against HepG-2 cell line (Figure 11).

Figure 11 summarised the SAR investigation of the newly synthesised compounds after their *in vitro* and *in silico* evaluation.

4. Conclusion

New series of pyrazolo[3,4-*d*]pyrimidine and pyrazolo[4,3-*e*][1,2,4]triazolo[1,5-*c*]pyrimidine compounds (**4–13**) and the thioglycoside derivatives (**14**, **15**) designed as novel CDK2 targeting compounds was synthesised. Most of the compounds showed superior cytotoxic activities against MCF-7 and HCT-116, and moderate activity against HepG-2 compared to Sorafenib. Compounds **14** and **15** showed the best cytotoxic activities against the three cell lines. Also, compounds **11**, **13**, **14**, and **15** revealed the most significant inhibitory activity against CDK2/cyclin A2. Compound

15 showed cell arrest at the S phase and apoptosis in Pre-G1 phase on HCT cells.

A molecular docking study revealed that all the potent anti-proliferative tested compounds were of comparable binding mode to that of the ligand. *In silico* ADMET studies and drug-likeness showed good pharmacokinetic properties of the new potent compounds. This helped in the prediction of structure requirements necessary for the observed antitumor activity.

5. Experimental

5.1. Chemistry

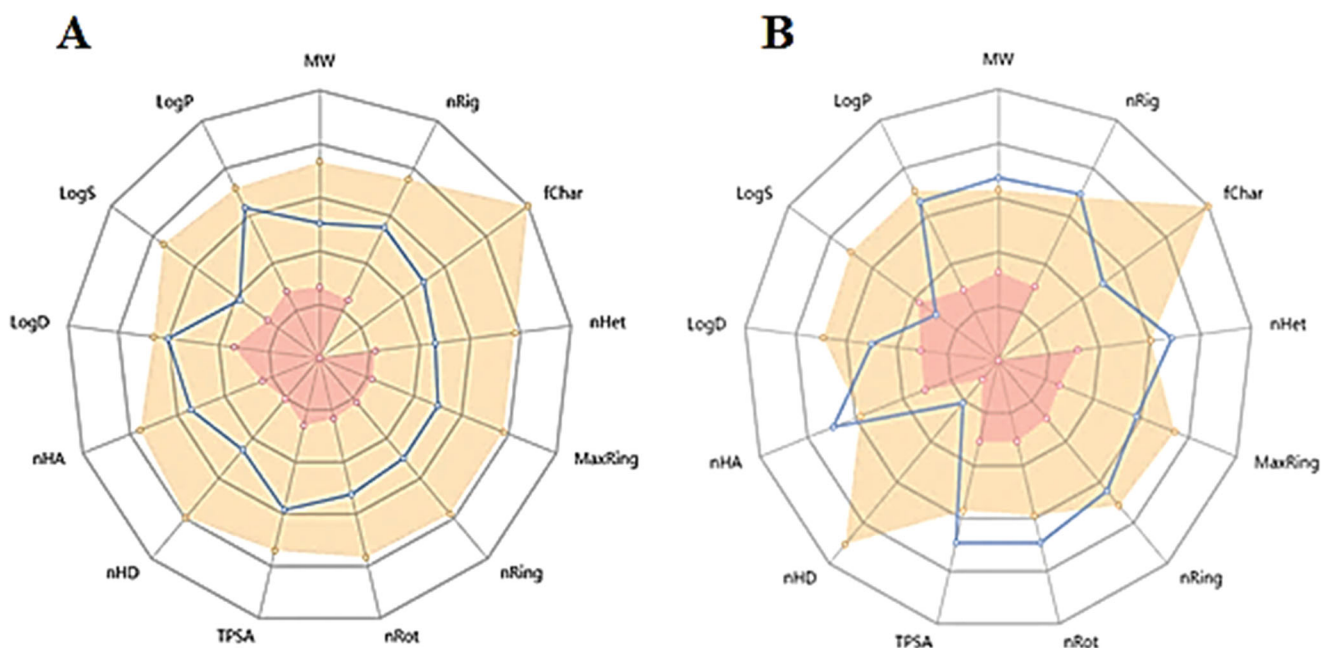
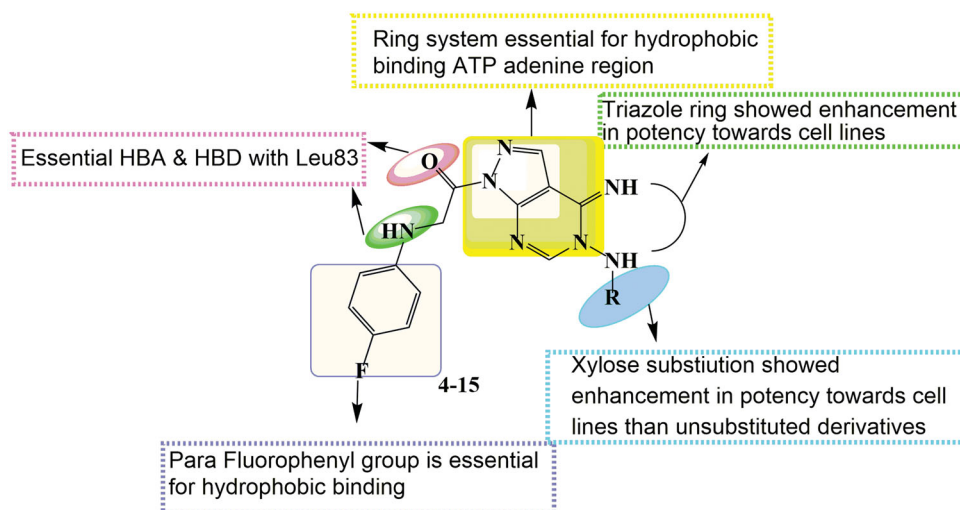
All melting points were measured using a Reichert Thermovar apparatus and are uncorrected. The IR spectra were recorded on a Perkin-Elmer model 1720 FTIR spectrometer for KBr disc. Routine NMR measurements were made on a JEOL ECA-500 II spectrometer with operating frequencies of 400 MHz for ¹H. Chemical shifts were reported in δ scale (ppm) relative to TMS as a reference standard and the coupling constants *J* values are given in Hz. ¹³C NMR were recorded at 125 MHz. The progress of the reactions was monitored by TLC using aluminium silica gel plates 60 F245. Spectral measurements and Elemental analyses were performed at the Micro-analytical centre at the Faculty of Science, Mansoura University, Mansoura. Compound **1** was synthesised according to a reported procedure⁴⁴.

5.1.1. 5-Amino-1-((4-fluorophenyl)glycyl)-1H-pyrazole-4-carbonitrile (**2**)

A solution of the acid hydrazide **1** (1.8 g, 10 mmol) and 2(ethoxymethylene)malononitrile (1.2 g, 10 mmole) in absolute ethanol (20 ml) was refluxed for 6 h, then cooled to room temperature. The resulted solid was recrystallized from ethanol to afford the pyrazole compound **2** as brown solid, yield 75%, m.p. 131–132 °C; IR (KBr): ν/cm^{-1} : 3340, 3255 (NH, NH₂), 2205 (CN), 1665 (C=O), 1620 (C=N); ¹H-NMR (DMSO-*d*₆) (ppm): 8.25 (s, 1H, pyrazolo-H3), 7.46 (brs, 1H, NH, D₂O exchangeable), 6.91 (d, *J* = 7.4 Hz, 2H, Ar-H), 6.55 (d, *J* = 7.4 Hz, 2H, Ar-H), 6.10 (brs, 2H, NH₂, D₂O exchangeable), 4.12 (s, 2H, CH₂); ¹³C NMR (DMSO-*d*₆) δ: (166.6), (158.6), (157.9), (145.4), (142.3), (131.6), (130.5), (126.4), (106.2), (54.1); MS (*m/z*): 259; Anal. Calc. for (C₁₂H₁₀FN₅O): C, 55.60; H, 3.89; N, 27.02%; Found C, C, 55.67; H, 3.95; N, 27.08%.

Table 8. ADMETlab absorption, distribution, and excretion parameters of the most potent compounds with promising docking results.

Name	Absorption						Distribution			Excretion	
	Caco-2	Pgp inh	Pgp sub	HIA	F20	F30	PPB	BBB	VD	T1/2	CL
8	-4.715	1	1	1	1	1	96.80	0	0.898	0.555	8.438 moderate
9	-4.647	1	1	1	1	1	97.15	0	0.977	0.218	9.419 moderate
11	-5.051	1	1	1	0	1	95.63	0	1.008	0.483	2.179 low
13	-4.77	1	1	1	1	1	96.21	0	1.372	0.365	5.718 moderate
14	-5.49	0	1	0	1	0	92.03	1	1.227	0.561	1.832 low
15	-5.49	0	1	0	1	0	92.03	1	1.227	0.561	1.832 low
Roscovitine	-4.343	1	0	0	1	1	30.14	0	1.143	0.844	9.767 moderate

**Figure 10.** The common physicochemical properties of compounds (A) Roscovitine, (B) Compound 15.**Figure 11.** Structure–activity relationship for compounds (4–15).

5.1.2. Ethyl -N-(4-cyano-1-((4-fluorophenyl)glycyl)-1H-pyrazol-5-yl) formimidate (3)

A mixture of the substituted pyrazole derivative **2** (2.6 g, 10 mmole) and triethyl orthoformate (1.4 g, 10 mmole) in acetic anhydride (20 ml) was heated under reflux for 6 h, then cooled

to room temperature. The precipitated formed was filtered and recrystallized by ethanol to afford the ester derivative **3** as Brown solid, yield 67%, m.p. 185–186 °C; IR (KBr): $\tilde{\nu}/\text{cm}^{-1}$: 3318 (NH), 2210 (CN), 1655 (C=O), 1620 (C=N); $^1\text{H-NMR}$ (DMSO- d_6) (ppm): 8.27 (s, 1H, pyrazolo-H3), 8.19 (s, 1H, N=CH), 7.42 (brs,

1H, NH, D₂O exchangeable), 6.91 (d, $J=7.4$ Hz, 2H, Ar-H), 6.52 (d, $J=7.4$ Hz, 2H, Ar-H), 4.13 (s, 2H, CH₂), 3.61 (q, $J=5.2$ Hz, 2H, CH₂), 1.2 (t, $J=5.2$ Hz, 3H, CH₃); ¹³C NMR (DMSO-*d*₆) δ : (166.3), (163.9), (159.4), (158.3), (147.2), (143.4), (131.9), (130.2), (126.4), (106.9), (64.2), (54.8), (18.3); MS (*m/z*): 315; Anal. Calc. for (C₁₅H₁₄FN₅O₂): C, 57.14; H, 4.48; N, 22.21%; Found C, 57.20; H, 4.52; N, 22.25%.

5.1.3. 1-(5-Amino-4-imino-4,5-dihydro-1H-pyrazolo[3,4-d]pyrimidin-1-yl)-2-((4-fluorophenyl)amino)ethan-1-one (4)

To solution of the ethyl ester derivative **3** (3.1 g, 10 mmol) in absolute ethanol (20 ml), hydrazine hydrate (99%, 1 ml, 20 mmol) was added dropwise. The reaction mixture was heated at reflux for 6 h then allowed to cool down to room temperature. The formed solid was separated by filtration and crystallised from methanol to provide the desired product as brown crystals (59%), m.p. = 168–169 °C; IR (KBr) cm⁻¹: 3350–3230 (NH₂, NH), 1660 (C=O), 1630 (C=N); ¹H-NMR (DMSO-*d*₆) (ppm): 11.42 (brs, 1H, NH, D₂O exchangeable), 8.77 (brs, 1H, NH, D₂O exchangeable), 8.51 (s, 1H, pyrimidine-H2), 7.98 (s, 1H, pyrazolo-H3), 7.56 (d, $J=8$ Hz, 2H, phenyl-H2,H6), 7.47 (d, $J=8$ Hz, 2H, phenyl-H3,H5), 5.51 (brs, 2H, NH₂, D₂O exchangeable), 4.12 (s, 2H, CH₂); ¹³C NMR (DMSO-*d*₆) δ : 168.7, 161.4, 153.5, 148.3, 143.1, 133.0, 129.4, 127.1, 122.2, 118.4, 55.9; MS (*m/z*) 301; Anal. Calc. for: (C₁₃H₁₂FN₇O): C, 51.83; H, 4.01; N, 32.54%; Found: C, 51.88; H, 4.05; N, 32.58%.

5.1.3.4. General procedure a. A mixture of aminopyrazolopyrimidine compound **4** (3 g, 10 mmol), the aldose sugar namely; D-glucose or D-xylose [10 mmol suspended in water (1 ml)] and glacial acetic acid (0.5 ml) in ethanol (25 ml) was allowed to be refluxed for 6 h. Half of the amount of the solvent was evaporated under reduced pressure and the resulting solution was cooled to room temperature and then left to stand in a refrigerator at 5–8 °C overnight. The resulting precipitated solid was filtered, dried, and recrystallized by methanol to afford the *N*-glycosyl compounds **5** or **6**, respectively.

5.1.4. 1-(4-Imino-5-((β -D-glucopyranosyl)amino)-4,5-dihydro-1H-pyrazolo[3,4-d]pyrimidin-1-yl)-2-((4-fluorophenyl)amino)ethan-1-one (5)

Brown solid, yield 66%, m.p. 183–184 °C; IR (KBr): ν /cm⁻¹: 3455–3440 (OH), 3325 (NH), 1668 (C=O), 1615 (C=N); ¹H-NMR (DMSO-*d*₆) (ppm): 11.25 (brs, 1H, NH, D₂O exchangeable), 8.74 (brs, 1H, NH, D₂O exchangeable), 8.51 (s, 1H, pyrimidine-H2), 7.79 (s, 1H, pyrazolo-H3), 7.60 (d, $J=8$ Hz, 2H, phenyl-H2,H6), 7.47 (d, $J=8$ Hz, 2H, phenyl-H3,H5), 6.71 (brs, 1H, NH, D₂O exchangeable), 5.10–5.13 (m, 1H), 4.97 (brs, 1H, OH, D₂O exchangeable), 4.66 (brs, 1H, OH, D₂O exchangeable), 4.63–4.62 (m, 2H), 4.43 (brs, 2H, 2OH, D₂O exchangeable), 4.13 (s, 2H, CH₂), 3.87–3.93 (m, 3H), 3.59–3.65 (m, 1H); ¹³C NMR (DMSO-*d*₆) δ : 169.0, 161.4, 155.5, 146.8, 143.0, 134.3, 128.8, 127.1, 122.5, 118.3, 93.0, 83.6, 75.7, 72.2, 71.8, 62.1, 55.5; MS (*m/z*) 463; Anal. Calc. for: (C₁₉H₂₂FN₇O₆): C, 49.24; H, 4.79; N, 21.16%; Found: C, 49.31; H, 4.84; N, 21.20%.

5.1.5. 1-(4-Imino-5-((β -D-xylopyranosyl)amino)-4,5-dihydro-1H-pyrazolo[3,4-d]pyrimidin-1-yl)-2-((4-fluorophenyl)amino)ethan-1-one (6)

Brown solid, yield 72%, m.p. 122–123 °C; IR (KBr): ν /cm⁻¹: 3460–3450 (OH), 3325 (NH), 1668 (C=O), 1622 (C=N); ¹H-NMR (DMSO-*d*₆) (ppm): 11.25 (brs, 1H, NH, D₂O exchangeable), 8.72

(brs, 1H, NH, D₂O exchangeable), 8.51 (s, 1H, pyrimidine-H2), 8.02 (s, 1H, pyrazolo-H3), 7.58 (d, $J=8$ Hz, 2H, phenyl-H2,H6), 7.47 (d, $J=8$ Hz, 2H, phenyl-H3,H5), 6.68 (brs, 1H, NH, D₂O exchangeable), 5.08–5.10 (m, 1H), 4.83 (brs, 1H, OH, D₂O exchangeable), 4.43 (brs, 2H, 2OH, D₂O exchangeable), 4.12 (s, 2H, CH₂), 3.90–3.96 (m, 2H), 3.71–3.76 (m, 3H); ¹³C NMR (DMSO-*d*₆) δ : 168.7, 161.4, 155.4, 146.8, 143.0, 134.3, 128.8, 127.1, 122.5, 118.3, 93.0, 83.6, 75.7, 70.5, 62.1, 55.5; MS (*m/z*) 433; Anal. Calc. for: (C₁₈H₂₀FN₇O₅): C, 49.88; H, 4.65; N, 22.62%; Found: C, 49.95; H, 4.70; N, 22.67%.

5.1.6. 1-(2-Thioxo-2,3-dihydro-7H-pyrazolo[4,3-*e*][1,2,4]triazolo[1,5-*c*]pyrimidin-7-yl)-2-((4-fluorophenyl)amino)ethan-1-one (7)

To a well-stirred mixture of compound **4** (3 g, 10 mmol), potassium hydroxide (0.67 g, 12 mmol) in ethanol 25 (mL), carbon disulphide (0.4 ml, 12 mmol) was added dropwise over 30 min. The reaction mixture was heated in the water bath at 70 °C for 1 h and then refluxed for 10 h. The solvent was evaporated under a vacuum, then poured onto ice-cold water (50 ml) and the solution was acidified, the precipitate formed was filtered, washed with water, and dried. Crystallisation from ethanol gave the thione derivative **7** as yellow solid, yield 74%, m. p 178–179 °C; IR (KBr): ν /cm⁻¹: 3328–3310 (NH), 1670 (C=O), 1616 (C=N); ¹H-NMR (DMSO-*d*₆) (ppm): 11.66 (brs, 1H, NH, D₂O exchangeable), 8.96 (brs, 1H, NH, D₂O exchangeable), 8.50 (s, 1H, pyrimidine-H2), 8.13 (s, 1H, pyrazolo-H3), 7.59 (d, $J=8$ Hz, 2H, phenyl-H2,H6), 7.47 (d, $J=8$ Hz, 2H, phenyl-H3,H5), 4.12 (s, 2H, CH₂); ¹³C NMR (DMSO-*d*₆) δ : 176.4, 170.5, 161.7, 154.2, 146.5, 143.0, 131.2, 129.1, 127.1, 122.2, 118.3, 56.2; MS (*m/z*) 343; Anal. Calc. for: (C₁₄H₁₀FN₇OS): C, 48.98; H, 2.94; N, 28.56%; Found: C, 49.08; H, 3.01; N, 28.62%.

5.1.7. 2-((7-((4-Fluorophenyl)glycyl)-7H-pyrazolo[4,3-*e*][1,2,4]triazolo[1,5-*c*]pyrimidin-2-yl)thio)acetonitrile (8)

A mixture of **7** (3.4 g, 10 mmol), chloroacetonitrile (0.7 g, 11 mmol) and anhydrous potassium carbonate (1.4 g, 10 mmol) in dimethyl formamide (20 ml) was stirred for 8 h at room temperature. The reaction mixture was poured into ice-cold water (50 ml) with vigorous stirring for 30 min and the formed precipitate was filtered, dried and recrystallized from ethanol to give the nitrile derivative **8** as brown powder, yield 63%; m.p > 300 °C; IR (KBr): ν /cm⁻¹: 3315 (NH), 2218 (CN), 1655 (C=O), 1612 (C=N); ¹H-NMR (DMSO-*d*₆) (ppm): 8.74 (brs, 1H, NH, D₂O exchangeable), 8.50 (s, 1H, pyrimidine-H2), 8.0 (s, 1H, pyrazolo-H3), 7.58 (d, $J=8$ Hz, 2H, phenyl-H2,H6), 7.47 (d, $J=8$ Hz, 2H, phenyl-H3,H5), 4.54 (s, 2H), 4.12 (s, 2H, CH₂); ¹³C NMR (DMSO-*d*₆) δ : 169.8, 166.3, 161.4, 154.2, 146.8, 142.7, 131.2, 129.1, 127.1, 122.5, 118.06, 118.01, 54.5, 17.0; MS (*m/z*) 382; Anal. Calc. for: (C₁₆H₁₁FN₈OS): C, 50.26; H, 2.90; N, 29.31%; Found: C, 50.33; H, 2.98; N, 29.38%.

5.1.7.1. General procedure b. A solution of pyrazolopyrimidine derivative **7** (3.4 g, 10 mmol), chloro-acetaldehyde dimethyl acetal (10 mmol), or 3-chloropropane-1,2-diol, and anhydrous potassium hydroxide (0.67 g, 10 mmol) in ethanol (25 ml) were heated under reflux with stirring for 10 h. The solvent was evaporated under reduced pressure and ice-cold water was added to the remaining residue with continuous stirring to afford a precipitate which was filtered, dried, and recrystallized from ethanol-water mixture 1:1 to afford the dimethoxy product **9** and **10**, respectively.

5.1.8. 1-(2-((2,2-Dimethoxyethyl)thio)-7H-pyrazolo[4,3-e][1,2,4]triazolo[1,5-c]pyrimidin-7-yl)-2-((4-fluorophenyl)amino)ethan-1-one (9)
Pale yellow solid, yield 65%, m.p. 190–192 °C; IR (KBr): ν/cm^{-1} : 3295 (NH), 1668 (C=O), 1618 (C=N); $^1\text{H-NMR}$ (DMSO- d_6) (ppm): 8.74 (brs, 1H, NH, D₂O exchangeable), 8.50 (s, 1H, pyrimidine-H2), 8.0 (s, 1H, pyrazolo-H3), 7.60 (d, $J=8$ Hz, 2H, phenyl-H2,H6), 7.47 (d, $J=8$ Hz, 2H, phenyl-H3,H5), 4.87–4.90 (m, 1H, OCH), 4.12 (s, 2H), 3.65 (s, 6H), 3.09–3.12 (m, 2H, SCH₂); $^{13}\text{C NMR}$ (DMSO- d_6) δ : 169.8, 166.3, 159.7, 157.2, 146.8, 142.7, 131.9, 129.4, 127.1, 122.9, 118.8, 96.8, 67.3, 55.9, 35.3; MS (m/z) 431; Anal. Calc. for: (C₁₈H₁₈FN₇O₃S): C, 50.11; H, 4.21; N, 22.73%; Found: C, 50.17; H, 4.26; N, 22.78%.

5.1.9. 1-{2-[(2,3-Dihydroxypropyl)thio]-7H-pyrazolo[4,3-e][1,2,4]triazolo[1,5-c]pyrimidin-7-yl}-2-((4-fluorophenyl)amino)ethan-1-one (10)

Brown solid, yield 72%, m.p. > 300 °C; IR (KBr): ν/cm^{-1} : 3425 (OH), 3315 (NH), 1676 (C=O), 1622 (C=N); $^1\text{H-NMR}$ (DMSO- d_6) (ppm): 8.72 (brs, 1H, NH, D₂O exchangeable), 8.50 (s, 1H, pyrimidine-H2), 8.13 (s, 1H, pyrazolo-H3), 7.58 (d, $J=8$ Hz, 2H, phenyl-H2,H6), 7.47 (d, $J=8$ Hz, 2H, phenyl-H3,H5), 4.76 (brs, 1H, OH, D₂O exchangeable), 4.57 (brs, 1H, OH, D₂O exchangeable), 4.12 (s, 2H), 3.70–3.73 (m, 1H), 3.45–3.48 (m, 2H), 3.15–3.17 (m, 2H); $^{13}\text{C NMR}$ (DMSO- d_6) δ : 170.1, 166.3, 159.3, 155.2, 146.8, 142.7, 131.6, 129.4, 127.4, 122.2, 118.0, 71.2, 65.6, 55.5, 35.3; MS (m/z) 417; Anal. Calc. for: (C₁₇H₁₆FN₇O₃S): C, 48.92; H, 3.86; N, 23.49%; Found: C, 48.96; H, 3.89; N, 23.54%.

5.1.10. 3-((7-((4-Fluorophenyl)glycyl)-7H-pyrazolo[4,3-e][1,2,4]triazolo[1,5-c]pyrimidin-2-yl)thio)propane-1,2-diyl diacetate (11)

A mixture of compound **10** (4.1 g, 10 mmol) and acetic anhydride (5 ml) in pyridine (15 ml) was stirred at room temperature for 8 h then allowed to cool down to room temperature and poured on cold water (30 ml) with vigorous stirring for 2 h. The formed precipitate was filtered, washed with water then with potassium hydrogen carbonate and dried. Crystallisation from methanol afford the acetylated product as Brown solid, yield 73%, m.p. 260–262 °C; IR (KBr): ν/cm^{-1} : 3318 (NH), 1672 (C=O); $^1\text{H-NMR}$ (DMSO- d_6) (ppm): 8.80 (brs, 1H, NH, D₂O exchangeable), 8.50 (s, 1H, pyrimidine-H2), 8.07 (s, 1H, pyrazolo-H3), 7.60 (d, $J=8$ Hz, 2H, phenyl-H2,H6), 7.48 (d, $J=8$ Hz, 2H, phenyl-H3,H5), 4.32–4.37 (m, 1H), 4.12 (s, 2H), 3.42–3.48 (m, 2H), 3.12–3.22 (m, 2H), 2.20 (s, 6H); $^{13}\text{C NMR}$ (DMSO- d_6) δ : 172.2, 171.8, 169.7, 165.6, 159.0, 153.8, 146.8, 142.7, 131.2, 129.4, 127.4, 121.8, 115.2, 74.2, 67.7, 55.2, 37.1, 23.6, 17.3, 17.0; MS (m/z) 501; Anal. Calc. for: (C₂₁H₂₀FN₇O₅S): C, 50.30; H, 4.02; N, 19.55%; Found: C, 50.38; H, 4.09; N, 19.62%.

5.1.11. 1-(2-((2-Hydroxyethyl)thio)-7H-pyrazolo[4,3-e][1,2,4]triazolo[1,5-c]pyrimidin-7-yl)-2-((4-fluorophenyl)amino)ethan-1-one (12)

A solution of pyrazolopyrimidine derivative **7** (3.4 g, 10 mmol), 1-chloroethanol (0.8 g, 10 mmol) and anhydrous potassium hydroxide (0.67 g, 10 mmol) in ethanol (25 ml) was heated under reflux for 12 h. The solvent was evaporated under reduced pressure and ice-cold water was added to the remaining residue with continuous stirring to afford a precipitate which was filtered, dried and recrystallized from methanol-water mixture 1:1 to provide the hydroxyethoxy compound **12** as Brown solid, yield 65%, m.p. 199–200 °C; IR (KBr): ν/cm^{-1} : 3415 (OH), 3345 (NH), 1672 (C=O), 1618 (C=N); $^1\text{H-NMR}$ (DMSO- d_6) (ppm): 8.72 (brs, 1H, NH, D₂O exchangeable), 8.50 (s, 1H, pyrimidine-H2), 8.03 (s, 1H, pyrazolo-

H3), 7.58 (d, $J=8$ Hz, 2H, phenyl-H2,H6), 7.44 (d, $J=8$ Hz, 2H, phenyl-H3,H5), 4.81 (brs, 1H, OH, D₂O exchangeable), 4.12 (s, 2H), 3.68–3.71 (m, 2H), 3.48–3.51 (m, 2H); $^{13}\text{C NMR}$ (DMSO- d_6) δ : 170.1, 165.9, 159.4, 153.8, 146.5, 142.7, 131.2, 129.4, 127.1, 122.2, 115.3, 66.3, 55.2, 32.6; MS (m/z) 387; Anal. Calc. for: (C₁₆H₁₄FN₇O₂S): C, 49.61; H, 3.64; N, 25.31%; Found: C, 49.69; H, 3.71; N, 25.37%.

5.1.12. 2-((7-((4-Fluorophenyl)glycyl)-7H-pyrazolo[4,3-e][1,2,4]triazolo[1,5-c]pyrimidin-2-yl)thio)ethyl acetate (13)

To a mixture of compound **12** (3.8 g, 10 mmol) and acetic anhydride (5 ml) in pyridine (15 ml) was stirred at room temperature for 14 h then cooled to room temperature. Ice-cold water (35 ml) was added with vigorous stirring for 3 h. The formed precipitate was filtered, washed with water then with potassium hydrogen carbonate and dried. Crystallisation from methanol afford the acetylated products as brown powder, yield 67%, m.p. 172–173 °C; IR (KBr): ν/cm^{-1} : 3318 (NH), 1675 (C=O), 1620 (C=N); $^1\text{H-NMR}$ (DMSO- d_6) (ppm): 8.80 (brs, 1H, NH, D₂O exchangeable), 8.50 (s, 1H, pyrimidine-H2), 8.03 (s, 1H, pyrazolo-H3), 7.58 (d, $J=8$ Hz, 2H, phenyl-H2,H6), 7.44 (d, $J=8$ Hz, 2H, phenyl-H3,H5), 4.12 (s, 2H), 3.93–3.96 (m, 2H), 3.51–3.54 (m, 2H), 2.32 (s, 3H); $^{13}\text{C NMR}$ (DMSO- d_6) δ : 171.5, 169.4, 165.9, 159.7, 153.4, 146.1, 142.7, 131.2, 129.1, 127.1, 122.5, 115.3, 67.3, 55.5, 17.3; MS (m/z) 429; Anal. Calc. for: (C₁₈H₁₆FN₇O₃S): C, 50.35; H, 3.76; N, 22.83%; Found: C, 50.39; H, 3.79; N, 22.87%.

5.1.12.1. General procedure c. To a suspension of potassium hydroxide (0.67 g, 10 mmol) in water (1 ml), a solution of pyrazolopyrimidine derivative **7** (3.4 g, 10 mmol) in acetone (20 ml) was added with continuous stirring for about 15 min, then a solution of the glycosyl bromide namely; 2,3,4,6-tetra-*O*-acetyl- α -D-glucopyranosyl bromide or 2,3,4,6-tetra-*O*-acetyl- α -D-galactopyranosyl bromide (12 mmol) in acetone (10 ml) was added portion-wise and the resulting mixture was stirred at room temperature for 5 h. The solvent was evaporated under reduced pressure and the residue was washed with cold water (15 ml) to remove any remained inorganic substance. Extraction of the product with ethyl acetate (50 ml) followed by removal of the solvent afforded a solid material which was treated with petroleum ether/diethyl ether mixture 3:1 (30 ml) with stirring for 15 min for further purification. The formed solid product was filtered and dried to give compounds **14** or **15**, respectively.

5.1.13. 1-(2-((Tetra-*O*-acetyl-*D*-glucopyranosyl)thio)-7H-pyrazolo[4,3e][1,2,4]triazolo[1,5-c]pyrimidin-7-yl)-2-((4-fluorophenyl)amino)ethan-1-one (14)

Pale yellow solid, yield 79%, m.p. 168–169 °C; IR (KBr): ν/cm^{-1} : 3330 (NH), 1670 (C=O), 1740 (C=O), 1620 (C=N); $^1\text{H-NMR}$ (DMSO- d_6) (ppm): 8.66 (brs, 1H, NH, D₂O exchangeable), 8.50 (s, 1H, pyrimidine-H2), 7.98 (s, 1H, pyrazolo-H3), 7.58 (d, $J=8$ Hz, 2H, phenyl-H2,H6), 7.42 (d, $J=8$ Hz, 2H, phenyl-H3,H5), 5.71–5.76 (m, 1H), 5.01–5.07 (m, 2H), 4.29–4.34 (m, 3H), 4.12 (s, 2H), 3.68–3.73 (m, 1H), 2.23 (s, 12H); $^{13}\text{C NMR}$ (DMSO- d_6) δ : 173.6, 173.2, 171.8, 171.5, 169.4, 165.3, 159.4, 153.8, 146.1, 142.7, 131.6, 129.1, 127.1, 122.2, 115.6, 84.3, 80.8, 76.7, 71.5, 67.3, 63.1, 55.5, 18.7, 18.3, 17.7, 17.3; MS (m/z) 673; Anal. Calc. for: (C₂₈H₂₈FN₇O₁₀S): C, 49.92; H, 4.19; N, 14.56%; Found: C, 49.97; H, 4.25; N, 14.59%.

5.1.14. 1-(2-((Tetra-O-acetyl-D-galactopyranosyl)thio)-7H-pyrazolo [4,3e][1,2,4]triazolo[1,5-c]pyrimidin-7-yl)-2-((4-fluorophenyl)amino)ethan-1-one (15)

Pale yellow solid, yield 75%, m.p. 172–173 °C; IR (KBr): ν /cm⁻¹: 3325 (NH), 1745 (C=O), 1665 (C=O), 1620 (C=N); ¹H-NMR (DMSO-*d*₆) (ppm): 8.67 (brs, 1H, NH, D₂O exchangeable), 8.50 (s, 1H, pyrimidine-H2), 7.98 (s, 1H, pyrazolo-H3), 7.58 (d, *J*=8 Hz, 2H, phenyl-H2,H6), 7.44 (d, *J*=8 Hz, 2H, phenyl-H3,H5), 5.82–5.74 (m, 1H), 5.01–5.07 (m, 2H), 4.29–4.38 (m, 3H), 4.12 (s, 2H), 3.68–3.73 (m, 1H), 2.23 (s, 12H); ¹³C NMR (DMSO-*d*₆) δ : 173.6, 173.2, 171.8, 171.5, 169.4, 165.6, 159.4, 153.8, 146.1, 142.7, 131.6, 129.1, 127.1, 122.2, 115.6, 84.3, 80.8, 76.7, 71.5, 67.3, 63.1, 55.5, 18.7, 18.3, 17.7, 17.3; MS (*m/z*) 673; Anal. Calc. for: (C₂₈H₂₈FN₇O₁₀S): C, 49.92; H, 4.19; N, 14.56%; Found: C, 49.99; H, 4.27; N, 14.61%.

5.2. Biological assays

5.2.1. *In vitro* anti-proliferative activity

The *In vitro* cytotoxicity of all the newly synthesised compounds against three cancer cell lines named: Human breast adenocarcinoma (MCF-7) cell line, hepatocellular carcinoma (HepG-2), and colorectal carcinoma (HCT-116) were performed. Cells were purchased from the American Type Culture Collection (ATCC, Rockville, MD, USA) (Supplementary Material). Results were compared to the reference Sorafenib. Also, the *in vitro* cytotoxic effect of compound **15** against *WI-38* normal lung cells was compared to Staurosporine as a reference standard. The MTT assay was performed according to published procedure^{37,38}. Briefly, 5000–10,000 cells per well were plated in a 96-well plate and allowed for growth for 24 h, then treated with the media of increased concentrations of tested compounds in 100 μ l amount, complete growth medium was further mixed with 100 μ l for each compound per well for 48 h before the assay. Then, the media were withdrawn, and 100 μ l of MTT was added to each well, which was incubated for 4 h. The formed formazan crystals were solubilised by the addition of 100 μ l of dimethyl sulfoxide (DMSO) solution. The cell viability was evaluated by measuring the optical density (OD) per well of the developed purple colour using spectrophotometric determination at 570 nm using an ELISA microplate reader (Epic-2 C micro-plate reader, Bio Tek, VT, USA). The optical density of the produced colour was measured at 570 nm. The IC₅₀ values (the required concentration to inhibit cell viability by 50%) were calculated. The data was expressed as a percentage of control cells (100 percent of cell viability).

5.2.2. CDK2/cyclin A2 assay

The *In vitro* assay of CDK2/cyclin A2 protein kinase was carried out on all the synthesised compounds **4**, **5**, **6**, **7**, **8**, **9**, **10**, **11**, **12**, **13**, **14**, and **15**. The assay was proceeded in Egypt applying Kinase-Glo Plus luminescence kinase Assay kit (Promega)³⁹. The Protocol steps were applied by enzyme and substrate dilution. Where, 1 μ l of inhibitor, 5% DMSO, 2 μ l of the enzyme, and 2 μ l of substrate/ATP mix were added after ATP and inhibitors were diluted in Kinase Buffer. Incubation for 10 min at room temperature was allowed, then 5 μ l of Reagent ADP-GloTM was added and incubated for another 40 min. After that, an amount equivalent to 10 μ l of Kinase Detection Reagent was added to be incubated at room temperature for another 30 min. Luminescence was (where Integration time range 0.5–1 s). The luminescent signal is in direct relation to the present quantity of ATP and in inverse relation to the activity of the kinase enzyme.

5.2.3. Flow cytometry cell cycle analysis

The cell cycle analysis protocol was performed on compound **14** on HCT-116 cells. The test is based on the content of DNA measurement via staining using propidium iodide. Cells were first washed in PBS before being kept at 4 °C for 3 min through the dropwise using vortex addition of cold 70% ethanol, this is to avoid cell clumping and to ensure fixation as well. Then 50 μ l from a stock of 100 μ g/ml ribonuclease was added to selectively stain only DNA. Finally, an amount of 200 μ l from a stock solution of 50 μ g/ml of propidium iodide was added⁴⁰.

5.2.4. Flow cytometric analysis of apoptosis

Annexin V—FITC—apoptosis detection kit (PN IM3546) was used to detect apoptosis in treated cells. Flow cytometric analysis was further performed according to manufacturer protocol. Where HCT-116 cells were allowed to grow in a 25 cm³ flask until 70–80% confluence. Then HCT-116 cells were treated with compound **15** for 48 h followed by a wash in PBS and suspended in 1 \times binding buffer. One μ l of annexin V-FITC solution together with 5 μ l of dissolved PI were added to 100 μ l of cell suspensions, then incubated for 15 min in the dark. An aliquot of 400 μ l of ice-cold 1 \times binding buffer was gently added and mixed. The flow cytometric analysis method for the determination of the percentage of apoptotic cells was performed on a COULTER[®] EPICS[®] XLTM Flow Cytometer (USA)⁴¹.

5.3. Molecular modeling studies

A molecular docking study using CDocker protocol in Discovery Studio 4.0 Software was carried out. The targeted compounds were docked into the CDK2 active site. The X-ray crystallographic structure of CDK2 complexed with Roscovitine (PDB ID: 2A4L) was downloaded from PDB^{9,12}. The binding mode of the designed compounds was studied to explain their biological results and to detect the essential hydrogen bonding with Leu83. Where the best pose out of ten for each compound was selected compared to the ligand binding mode. *In silico* ADMET studies using Discovery Studio 4.0 Software and ADMETlab web tool were carried out to predict the pharmacokinetic properties of the targeted compounds⁴³, which helped in structure requirements prediction for the observed antitumor activity.

Acknowledgements

The authors extend their appreciation to the Research center at Al Maarefa University for funding this work. Acknowledgement for Future University in Egypt (FUE) Computer Aided Drug Design labs.

Disclosure statement

No potential conflict of interest was reported by the author(s).

Funding

This research did not receive any specific grant from funding agencies in the public, commercial, or not-for-profit sectors.

ORCID

Ibrahim F. Nassar  <http://orcid.org/0000-0002-8123-2238>

Wael A. El-Sayed  <http://orcid.org/0000-0002-8232-1830>
 Nasser S. M. Ismail  <http://orcid.org/0000-0002-5119-9318>

Data availability statement

Supporting data is supplied with the manuscript.

References

- Baillache DJ, Unciti-Broceta A. Recent developments in anticancer kinase inhibitors based on the pyrazolo [3,4-*d*] pyrimidine scaffold. *RSC Med Chem* 2020;11:1112–35. <https://pubs.rsc.org/en/content/articlelanding/2020/md/d0md00227e>
- Abdelgawad MA, Elkanzi NA, Nayl AA, et al. Targeting tumor cells with pyrazolo [3,4-*d*] pyrimidine scaffold: a literature review on synthetic approaches, structure activity relationship, structural and target-based mechanisms. *Arab J Chem* 2022;15:103781.
- Cohen P. Protein kinases—the major drug targets of the twenty-first century? *Nat Rev Drug Discov* 2002;1:309–15.
- Abd El-Sattar NE, Badawy EH, AbdEl-Hady WH, et al. Design and synthesis of new CDK2 inhibitors containing thiazolone and thiazolthione scaffold with apoptotic activity. *Chem Pharm Bull* 2021;69:106–17.
- Chen J, Pang L, Wang W, et al. Decoding molecular mechanism of inhibitor bindings to CDK2 using molecular dynamics simulations and binding free energy calculations. *J Biomol Struct Dyn* 2020;38:985–96.
- Liang SS, Liu XG, Cui YX, et al. Molecular mechanism concerning conformational changes of CDK2 mediated by binding of inhibitors using molecular dynamics simulations and principal component analysis. *SAR QSAR Environ Res* 2021;32:573–94.
- Kontopidis G, McInnes C, Pandalaneni SR, et al. Differential binding of inhibitors to active and inactive CDK2 provides insights for drug design. *Chem Biol* 2006;13:201–11.
- Li Y, Zhang J, Gao W, et al. Insights on structural characteristics and ligand binding mechanisms of CDK2. *Int J Mol Sci* 2015;16:9314–40.
- Husseiny EM. Synthesis, cytotoxicity of some pyrazoles and pyrazolo[1,5-*a*]pyrimidines bearing benzothiazole moiety and investigation of their mechanism of action. *Bioorg Chem* 2020;102:104053.
- Wee S, Dhanak D, Li H, Armstrong, et al. Targeting epigenetic regulators for cancer therapy. *Ann N Y Acad Sci* 2014;1309:30–6.
- Cherukupalli S, Karpoornath R, Chandrasekaran B, et al. An insight on synthetic and medicinal aspects of pyrazolo [1,5-*a*] pyrimidine scaffold. *Eur J Med Chem* 2017;126:298–352.
- Ali GM, Ibrahim DA, Elmetwali AM, et al. Design, synthesis and biological evaluation of certain CDK2 inhibitors based on pyrazole and pyrazolo [1,5-*a*] pyrimidine scaffold with apoptotic activity. *Bioorg Chem* 2019;86:1–4.
- Farag AM, Fahim AM. Synthesis, biological evaluation and DFT calculation of novel pyrazole and pyrimidine derivatives. *J Mol Struct* 2019;1179:304–14.
- Gökhan-Keleşçi N, Yabanoğlu S, Küpeli E, et al. A new therapeutic approach in Alzheimer disease: some novel pyrazole derivatives as dual MAO-B inhibitors and antiinflammatory analgesics. *Bioorg Med Chem* 2007;15:5775–86.
- Nithyabalaji R, Krishnan H, Sribalan R. Synthesis, molecular structure and multiple biological activities of *N*-(3-methoxyphenyl)-3-(pyridin-4-yl)-1*H*-pyrazole-5-carboxamide. *J Mol Struct* 2019;1186:1–10.
- Hernández-Vázquez E, Salgado-Barrera S, Ramírez-Espinosa JJ, et al. Synthesis and molecular docking of *N'*-arylidene-5-(4-chlorophenyl)-1-(3,4-dichlorophenyl)-4-methyl-1*H*-pyrazole-3-carbohydrazides as novel hypoglycemic and antioxidant dual agents. *Bioorg Med Chem* 2016;24:2298–306.
- Nassar IF, El Farargy AF, Abdelrazek FM, et al. Design, synthesis and anticancer evaluation of novel pyrazole, pyrazolo [3,4-*d*] pyrimidine and their glycoside derivatives. *Nucleosides Nucleotides Nucleic Acids* 2017;36:275–91.
- Nassar IF, Atta-Allah SR, Elgazwy AS. A convenient synthesis and molecular modeling study of novel pyrazolo[3,4-*d*]pyrimidine and pyrazole derivatives as anti-tumor agents. *J Enzyme Inhib Med Chem* 2015;30:396–405.
- Rashad AE, Mahmoud AE, Ali MM. Synthesis and anticancer effects of some novel pyrazolo [3,4-*d*] pyrimidine derivatives by generating reactive oxygen species in human breast adenocarcinoma cells. *Eur J Med Chem* 2011;46:1019–26.
- Hassan GS, Kadry HH, Abou-Seri SM, et al. Synthesis and *in vitro* cytotoxic activity of novel pyrazolo [3,4-*d*] pyrimidines and related pyrazole hydrazones toward breast adenocarcinoma MCF-7 cell line. *Bioorg Med Chem* 2011;19:6808–17.
- El-Naggar M, Hassan AS, Awad HM, et al. Design, synthesis and antitumor evaluation of novel pyrazolopyrimidines and pyrazoloquinazolines. *Molecules* 2018;23:1249.
- Radi M, Dreassi E, Brullo C, et al. Design, synthesis, biological activity, and ADME properties of pyrazolo [3,4-*d*] pyrimidines active in hypoxic human leukemia cells: a lead optimization study. *J Med Chem* 2011;54:2610–26.
- Curran KJ, Verheijen JC, Kaplan J, et al. Pyrazolopyrimidines as highly potent and selective, ATP-competitive inhibitors of the mammalian target of rapamycin (mTOR): optimization of the 1-substituent. *Bioorg Med Chem Lett* 2010;20:1440–4.
- Li Y, Gao W, Li F, et al. An *in silico* exploration of the interaction mechanism of pyrazolo [1,5-*a*] pyrimidine type CDK2 inhibitors. *Mol Biosyst* 2013;9:2266–81.
- Almehmadi SJ, Alsaedi AM, Harras MF, et al. Synthesis of a new series of pyrazolo[1,5-*a*]pyrimidines as CDK2 inhibitors and anti-leukemia. *Bioorg Chem* 2021;117:105431.
- Ismail NS, Ali EM, Ibrahim DA, et al. Pyrazolo [3,4-*d*] pyrimidine based scaffold derivatives targeting kinases as anti-cancer agents. *Future J Pharm Sci* 2016;2:20–30.
- Chauhan M, Kumar R. Medicinal attributes of pyrazolo[3,4-*d*]pyrimidines: a review. *Bioorg Med Chem* 2013;21:5657–68.
- Schenone S, Radi M, Musumeci F, et al. Biologically driven synthesis of pyrazolo[3,4-*d*]pyrimidines as protein kinase inhibitors: an old scaffold as a new tool for medicinal chemistry and chemical biology studies. *Chem Rev* 2014;114:7189–238.
- Bocci G, Fioravanti A, La Motta C, et al. Antiproliferative and proapoptotic activity of CLM3, a novel multiple tyrosine kinase inhibitor, alone and in combination with SN-38 on endothelial and cancer cells. *Biochem Pharmacol* 2011;81:1309–16.
- Abdelgawad MA, Bakr RB, Alkhoja OA, et al. Design, synthesis and antitumor activity of novel pyrazolo [3,4-*d*] pyrimidine derivatives as EGFR-TK inhibitors. *Bioorg Chem* 2016;66:88–96.
- Le Brazidec JY, Pasis A, Tam B, et al. Synthesis, SAR and biological evaluation of 1,6-disubstituted-1*H*-pyrazolo[3,4-

- d*]pyrimidines as dual inhibitors of Aurora kinases and CDK1. *Bioorg Med Chem Lett* 2012;22:2070–4.
32. Cherukupalli S, Chandrasekaran B, Aleti RR, et al. Synthesis of 4, 6-disubstituted pyrazolo [3,4-*d*] pyrimidine analogues: cyclin-dependent kinase 2 (CDK2) inhibition, molecular docking and anticancer evaluation. *J Mol Struct* 2019;1176:538–51.
 33. Rahmouni A, Souiei S, Belkacem MA, et al. Synthesis and biological evaluation of novel pyrazolopyrimidines derivatives as anticancer and anti-5-lipoxygenase agents. *Bioorg Chem* 2016;66:160–8.
 34. Cherukupalli S, Chandrasekaran B, Kryštof V, et al. Synthesis, anticancer evaluation, and molecular docking studies of some novel 4,6-disubstituted pyrazolo[3,4-*d*]pyrimidines as cyclin-dependent kinase 2 (CDK2) inhibitors. *Bioorg Chem* 2018;79:46–59.
 35. Elgazwy AS, Ismail NS, Elzahabi HS. A convenient synthesis and molecular modeling study of novel purine and pyrimidine derivatives as CDK2/cyclin A3 inhibitors. *Bioorg Med Chem* 2010;18:7639–50.
 36. Abdel-Aal MT, El-Sayed WA, El-Kosy SM, et al. Synthesis and antiviral evaluation of novel 5-(*N*-aryl-aminomethyl-1,3,4-oxadiazol-2-yl) hydrazines and their sugars, 1,2,4-triazoles, tetrazoles and pyrazolyl derivatives. *Arch Pharm Chem Life Sci* 2008;341:307–13.
 37. Girgis AS, Stawinski J, Ismail NS, et al. Synthesis and QSAR study of novel cytotoxic spiro[3*H*-indole-3,2'(1'*H*)-pyrrolo[3,4-*c*]pyrrole]-2,3',5' (1*H*,2'*aH*,4'*H*)-triones. *Eur J Med Chem* 2012; 47:312–22.
 38. Fawzy IM, Youssef KM, Lasheen DS, et al. Design, synthesis and 3D QSAR based pharmacophore study of novel imatinib analogs as antitumor-apoptotic agents. *Future Med Chem* 2018;10:1421–33.
 39. Hennek J, Alves J, Yao E, et al. Bioluminescent kinase strips: a novel approach to targeted and flexible kinase inhibitor profiling. *Anal Biochem* 2016;495:9–20.
 40. Pozarowski P, Darzynkiewicz Z. Analysis of cell cycle by flow cytometry. In: Checkpoint controls and cancer. Humana Press; 2004. p. 301–11. doi:10.1385/1-59259-811-0:301.
 41. Ismail A, Doghish AS, Elsadek BE, et al. Hydroxycitric acid potentiates the cytotoxic effect of tamoxifen in MCF-7 breast cancer cells through inhibition of ATP citrate lyase. *Steroids* 2020;160:108656.
 42. Bitew M, Desalegn T, Demissie TB, et al. Pharmacokinetics and drug-likeness of antidiabetic flavonoids: molecular docking and DFT study. *PLoS One* 2021;16:e0260853.
 43. Dong J, Wang NN, Yao ZJ, et al. ADMETlab: a platform for systematic ADMET evaluation based on a comprehensively collected ADMET database. *J Cheminformatics* 2018;10:1.
 44. Zou W, Ma X, Hua W, et al. BRIP1 inhibits the tumorigenic properties of cervical cancer by regulating RhoA GTPase activity. *Oncol Lett* 2016;11:551–8.